ISSN 1999-656X

Iraqi Journal of Applied Physics Letters

VOLUME (5) ISSUE (2) APRIL-JUNE 2022

Sponsored and Published by
Iraqi Society for Alternative and Renewable Energy Sources and Techniques

Co-published by
American Quality for Scientific Publishing

IRAQI JOURNAL OF APPLIED PHYSICS LETTERS

The *Iraqi Journal of Applied Physics Letters (IJAPLett)* is a peer reviewed journal of high quality devoted to the publication of original research papers from applied physics and their broad range of applications. IJAPLett publishes quality original research letters in physics and its applications in the broadest sense. It is intended that the journal may act as an interdisciplinary forum for physics and its applications. Innovative applications and material that brings together diverse areas of physics are particularly welcome. IJAPLett aims to disseminate knowledge; provide a learned reference in the field; and establish channels of communication between academic and research experts, policy makers and executives in industry, commerce and investment institutions. IJAPLett is a quarterly specialized periodical dedicated to publishing original letters in: Applied & Nonlinear Optics, Applied Mechanics & Thermodynamics, Digital & Optical Communications, Electronic Materials & Devices, Laser Physics & Applications, Plasma Physics & Applications, Quantum Physics & Spectroscopy, Semiconductors & Optoelectronics, Solid State Physics & Applications, Alternative & Renewable Energy, and Environmental Science & Technology.

ISSN (Print): 1999-656X, ISSN (Online): 2958-6488

EDITORIAL BOARD

Editorial Office:
P. O. Box 55259, Baghdad 12001, IRAQ
Website: www.iraqiphysicsjournal.com
Emails: editor@iraqiphysicsjournal.com, editor_ijap@yahoo.co.uk, ijap.editor@gmail.com,

ADVISORY BOARD

SPONSORED BY
IRAQI SOCIETY FOR ALTERNATIVE AND RENEWABLE ENERGY SOURCES AND TECHNIQUES (I.S.A.R.E.S.T.)
P. O. Box 55259, Baghdad 12001, IRAQ

PUBLISHED BY
AMERICAN QUALITY FOR SCIENTIFIC PUBLISHING INC.
1479 South De Gaulle Ct, Aurora,
CO 80018, United States

IRAQI JOURNAL OF APPLIED PHYSICS LETTERS

ISSN (Print): 1999-656x, ISSN (Online): 2309-1673

INSTRUCTIONS TO AUTHORS

CONTRIBUTIONS

Contributions to be published in this journal should be original research letters, i.e., those not already published or submitted for publication elsewhere, communications or letters to editor.
Manuscripts should be submitted to the editor at the mailing address:

Iraqi Journal of Applied Physics Letters, Editorial Board, P. O. Box 55259, Baghdad 12001, IRAQ
Website: www.iraqiphysicsjournal.com
Email: editor@iraqiphysicsjournal.com, editor_ijap@yahoo.co.uk, ijap.editor@gmail.com

MANUSCRIPTS

Two hard copies with soft Word copy on a CD or DVD should be submitted to Editor in the following configuration:

- **One-column** Double-spaced one-side A4 size with 2.5 cm margins of all sides
- Times New Roman font (16pt bold for title, 14pt bold for names, 12pt bold for headings, 12pt regular for text)
- Manuscripts presented in English only are accepted.
- Total number of words not exceed 2500 words and English abstract not exceed 100 words
- 4 keywords (at least) should be maintained on (PACS preferred)
- Author(s) should express all quantities in SI units
- Equations should be written in equation form (*italic* and symbolic) NOT in plain text
- Tables and Figures should be separated from text and placed in new pages after the references
- Charts should be indicated by the software used for generating them (e.g., Excel, MATLAB, Grapher, etc.)
- Figures and diagrams can be submitted in original colored forms for assessment and they will be returned to authors after provide printable copies
- Only original or high-resolution scanner photos are accepted
- For electronic submission, articles should be formatted with MS-Word software.

AUTHOR NAMES AND AFFILIATIONS

It is IJAPLett policy that all those who have participated significantly in the technical aspects of a paper be recognized as co-authors or cited in the acknowledgments. In the case of a paper with more than one author, correspondence concerning the paper will be sent to the first author unless staff is advised otherwise.
Author name should consist of first name, middle initial, last name. The author affiliation should consist of the following, as applicable, in the order noted:
- Company or college (with department name or company division), Postal address, City, Governorate or State, zip code, Country name, contacting telephone number, and e-mail

REFERENCES

The references should be brought at the end of the article, and numbered in the order of their appearance in the paper. The reference list should be cited in accordance with the following examples:
[1] X. Ning, R. Benford and M.R. Lovell, "On the Sliding Friction Characteristics of Unidirectional Continuous FRP Composites", *J. Tribol. Func. Mater.*, 124(1) (2002) 5-13.
[2] M. Barnes, "Stresses in Solenoids", *J. Appl. Phys.*, 48(5) (2001) 2000–2008.
[3] J. Jones, **"Contact Mechanics"**, Cambridge University Press (Cambridge, UK) (2000), Ch.6, p.56.
[4] Y. Lee, S.A. Korpela and R. Horne, "Structure of Multi-Cellular Natural Convection in a Tall Vertical Annulus", Proceedings of 7th International Heat Transfer Conference, U. Grigul et al., eds., Hemisphere (Washington DC), 2 (1982) 221–226.
[5] M. Hashish, "Waterjet Technology Development", High Pressure Technology, PVP-Vol. 406 (2000) 135-140.
[6] D.W. Watson, "Thermodynamic Analysis", ASME Paper No. 97-GT-288 (1997).
[7] C.Y. Tung, "Evaporative Heat Transfer in the Contact Line of a Mixture", Ph.D. thesis, Rensselaer Polytechnic Institute, Troy, NY (1982).

PROOFS

Authors will receive proofs of papers and are requested to return one corrected copy as a WORD file on a compact disc (CD) or by email. New materials inserted in the original text without Editor's permission may cause rejection of paper unless the handling editor is informed.

COPYRIGHT FORM

Author(s) will be asked to sign the IJAPLett Copyright Form and hence transfer copyrights of the article to the Journal soon after acceptance of it. This will ensure the widest possible dissemination of information.

OFFPRINTS

Authors will receive electronic offprint free of charge and any additional reprints can be ordered.

SUBSCRIPTION AND ORDERS

Annual fees (4 issues per year) of subscription are:
50 US$ for individuals inside Iraq; **200** US$ for institutions inside Iraq;
100 US$ for individuals abroad; **300** US$ for institutions abroad.

Spectroscopic Characteristics of Biosynthesized Silver Nanoparticles Using Ruta Leaf Extract

Muataz A. Majeed[1], Souad G. Khalil[2], Ghasan A. Naeem[3]

[1] Salahaldeen Education Directorate, Ministry of Education, IRAQ
[2] Department of Physics, College of Science, Baghdad University, Baghdad, IRAQ
[3] Department of Medical Physics, College of Applied Science-Hit, University of Anbar, Hit, Anbar, IRAQ

Abstract
The purpose of this study is to optimize the green synthesis of AgNPs using various quantity of Ruta leaf extracts, the biosynthesized AgNPs were characterized using UV–visible and FTIR spectroscopy. The examination of the visible and ultraviolet spectra revealed an absorption peak in the region of 405-420 nm. Through the use of FTIR spectroscopy, the functional groups that were found in the Ruta plant extract were analyzed in order to locate the components that were accountable for reducing the silver nitrate.

Keywords: Nanotechnology; Ruta leaf; Zeta potential; EDX analysis; Biological method
Received: 1 April 2021; **Revised:** 5 June 2021; **Accepted:** 9 September 2021; **Published:** 1 March 2022

1. Introduction

The production of nanoparticles may be performed by a number of methods, some of which include biological, chemical, and physical methods [1-3]. Green synthesis has attracted significant attention as an environmentally friendly, low cost, energy efficient and non-toxic method for preparing silver anoparticles (AgNPs) [4]. Green chemistry focuses on liminating or minimizing the use of toxic chemicals [5]. In order to achieve this goal, the strategy makes use of chemical catalysts. The production of nanoparticles calls for the incorporation of a wide range of chemicals, including those with reducing and stabilizing properties. Phytochemicals in plants, such as polyphenols, flavonoids, tannins, proteins, and sugars, are responsible for synthesizing nanoparticles and serve as reducing and stabilizing agents [6]. However, the make-up of these components may be different based on the kind of plant that was extracted, the plant section that was extracted, and the method that was used to extract the plant. Because of this, the amount of extract that is used in the reaction has a substantial influence on the technique that is used to prepare the substance [7]. When the biological material that is used in the preparation of nanoparticles is increased in concentration, higher contents of the biomolecules that are involved in the process of metal reduction become available. This is because the concentration of the biological material is directly proportional to the amount of biomolecules that are present [8].

2. Materials and Methods

The leaves of the Ruta plant, which were utilized in the production of silver nanoparticles, were obtained from a farm in Kabisa, which is located in Anbar Province in Iraq. The British company Sigma-Aldrich provided silver with a purity level of 99.9%, which was used in the experiment.

After being washed thoroughly with distilled water, the leaves were dried in an electric oven. An electric blender was used to pulverize the dry leaves. To 4 grams of leaf powder, 200 milliliters of distilled water were added. The resulting mixture was heated to 90 degrees Celsius for twenty minutes while being continuously stirred. Whatman filter paper was then used to filter the material that was extracted from the leaves. The extract was stored at a temperature of 3 degrees Celsius until it was required.

Both an aqueous solution of silver nitrate ($AgNO_3$) with a concentration of one millimolar and leaf extracts with concentrations ranging from 0.5 to 1.75

milliliters were generated separately. The leaf extracts ranged in concentration from 0.5 to 1.75 milliliters. The amount of the extract needed to be adjusted as a result of the use of Ruta leaf extract in a variety of different sizes. The amounts of the extract were as follows: (0.5, 0.75, 1, 1.25, 1.5, and 1.75 ml). Following the preparation of 20 mL of a solution of $AgNO_3$ with a concentration of 1 mM, each amount of leaf extract was added. After fifteen minutes, the color of the solution changes from a light yellow to a brownish hue, which is a sign that AgNPs have been formed. This change in hue is indicative of the production of AgNPs.

the analytical methods that have been used in the process of analyzing the properties of AgNPs are: Ultraviolet-visible spectroscopy (NOVIALAB, UV-visible 1911 DB spectrometer) was used to investigate the formation of silver nanoparticles in colloidal solution and study the optical properties of the synthesized silver nanoparticles. FTIR spectrometer (BRUKER FTIR spectrophotometer, Platinum ATR) is used to identify and evaluate functional or active groups of chemical compounds in the plant extract separately and for silver nanoparticles and plant extract together.

3. Results and Discussion

As can be seen in Fig. (1), after a period of 15 minutes has elapsed since the beginning of the reaction, the color of the solution that is being used in the reaction has transformed from being colorless to yellow. Brown is the new hue after an hour and a half has elapsed since the transition began. The progressive increase in color intensity that has been seen over time is due to the activation of surface plasmon vibrations in the metallic nanoparticles [8]. This is responsible for the gradual rise in color intensity. In order to confirm the creation of biosynthesized silver nanoparticles, UV-Vis (NOVIALAB UV-visible 1911 DB spectrometer) measurements were carried out, and the following quantities of each component were used in the experiment: 0.01 mL, 0.02 mL, 0.04 mL, 0.06 mL, and 0.08 mL. (0.5, 0.75, 1, 1.25, 1.5, 1.75 ml). The increase in absorbance that we see in Fig. 1 as a result of an increase in the size of the extract is an indication of an increase in the production of silver nanoparticles [9]. This can be seen by looking at the graph. Our interpretation of this occurrence leads us to believe that there has been an uptick in the production of silver nanoparticles. We find that there is a direct correlation between the volume of the extract and the quantity of biomolecules that are readily available to take part in the process of silver reduction. This is something that we have seen. The end effect is a hue that has a deeper saturation. This effect has been described with banana peel extract [8]. So that enhanced absorbency occurs with increasing extract volume it is consistent with [10].

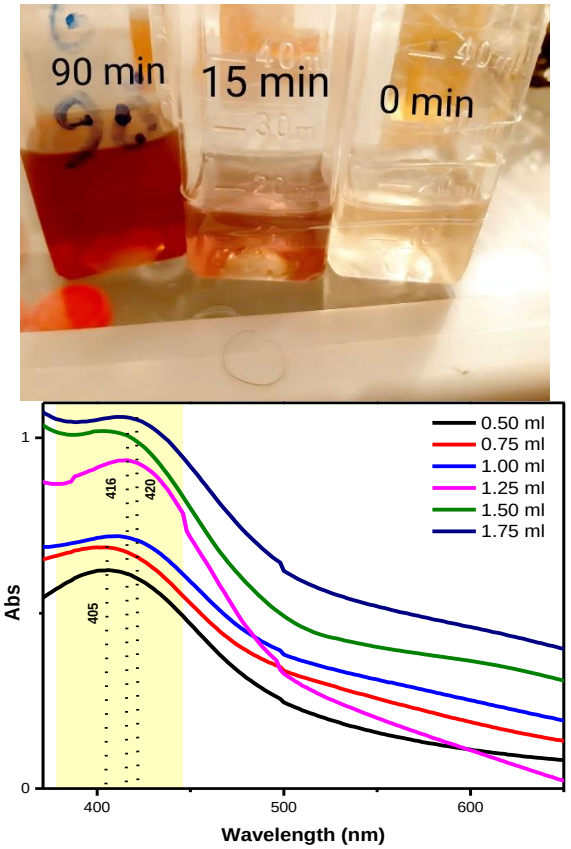

Fig. (1) Color change and UV-visible spectroscopy of AgNPs when using different extract sizes

A spectrophotometric study using BRUKER Platinum ATR Fourier-transform infrared (FTIR) spectrophotometer was carried out in order to evaluate the chemical composition of the plant extract and the

effective groups that were present in the extract. The results of this study are depicted in Fig. (2), and they show how the effective groups were distributed throughout the extract. We take note of the fact that there is a resemblance in the positions of the beams and, more importantly, in the positions in figure where the infrared spectrum of the plant extract was shown (Fig. 2a) The presence of a group (O=C-N-H) that binds two consecutive amino acids may be deduced from the observation of an absorption beam at a wavelength of 580 cm^{-1} in the extract of the protein or peptide. This can be done by looking at the structure of the protein or peptide. An absorption beam with a frequency of 1637 cm^{-1} is produced when there is a stretching vibration of carbon dioxide to oxygen, which is present in the structure of flavonoids, peptides, amino acids, and proteins. This vibration is responsible for the occurrence of an absorption beam. The absorption band that occurs at a wavelength that ranges from 3150-3350 cm^{-1} may be used to identify whether or not the group ($-NH_2$) is present during the process of creating proteins and amino acids. The stretch vibration of the absorption beam at 3253 cm^{-1} reveals that the plant extract contains peptides, flavonoids, amino acids, proteins, carbs, and polyphenols. Additionally, this vibration indicates that there is a presence of carbohydrates. The presence of the carboxyl group (-COOH) in monosaccharides may be shown by the observation of a wide absorption band that has a range that extends from 2520 to 3600 cm^{-1}. As an additional piece of evidence for the existence of this group, the presence of the carboxyl group (-COOH) in peptides, amino acids, and proteins all provide support for this assertion. Figure (2b) displays the FTIR spectroscopy of silver nanoparticles that were manufactured using biofabrication. It was discovered that the spectrum of the nanomaterials is very equivalent to the spectral range of the extract from the plant Ruta, with the exception of one clear band that is located in 2100-2200 cm^{-1}, and that band belongs to the CO of phenols, amines, carboxylic, proteins, and peptides [11-18].

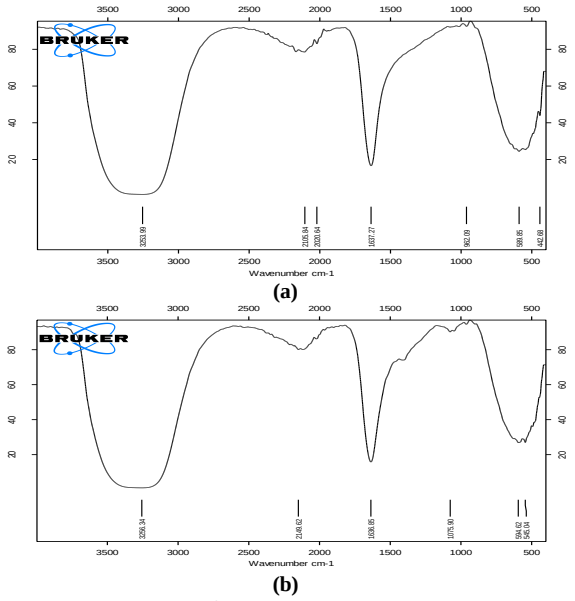

Fig. (2) FTIR spectra of (a) Ruta extract, and (b) Ruta extract with AgNPs

4. Conclusion

Green synthesis of AgNPs using Ruta leaf extract was performed, and AgNPs with well-defined morphologies were created. the results showed that the various quantity of Ruta leaf extracts had substantial effects on the green synthesis of the AgNPs. Based on the results of the current study, the FTIR analysis revealed the presence of some functional groups (O=C-N-H), ($-NH_2$),(-COOH), and (C-O) and confirmed that the bio-compounds: amino acids, proteins, peptides, phenols, amines, carboxylic, and peptides, present in the plant extracts were adsorbed on the surface of the AgNPs, thus enhancing their properties. This study focused on the green synthesis of AgNPs using different amounts of rota leaf extracts which induced the formation of AgNPs with well-defined sizes and shapes, thus improving the properties of the nanoparticles.

References

[1] E. Pauwels et al., "Nanoparticles in cancer", *Curr. Radiopharma.*, 1(1) (2008) 30-36.

[2] W.P. Hall, S.N. Ngatia and R.P. van Duyne, "LSPR biosensor signal enhancement using nanoparticle-antibody conjugates", *J. Phys. Chem. C*, 115(5) (2011) 1410-1414.

[3] H. Kato, "In vitro assays: tracking nanoparticles inside cells", *Nature Nanotechnol.*, 6(3) (2011) 139-140.

[4] K. Gudikandula and S. Charya Maringanti, "Synthesis of silver nanoparticles by chemical and biological methods and their antimicrobial properties", *J. Exp. Nanosci.*, 11(9) (2016) 714-721.
[5] M. Ndikau et al., "Green Synthesis and Characterization of Silver Nanoparticles Using Citrullus lanatus Fruit Rind Extract", *Int. J. Anal. Chem.*, 2017, Article ID 8108504.
[6] B.V. Badami, "Concept of green chemistry", *Resonance*, 13(11) (2008) 1041-1048.
[7] J. Kumar Patra and K.-H. Baek, "Green Nanobiotechnology: Factors Affecting Synthesis and Characterization Techniques", *J. Nanomater.*, 2014, Article ID 417305.
[8] H.M.M. Ibrahim, "Green synthesis and characterization of silver nanoparticles using banana peel extract and their antimicrobial activity against representative microorganisms", *J. Rad. Res. Appl. Sci.*, 8(3) (2015) 265-275.
[9] N.W. Mamdooh and G.A. Naeem, "Green Synthesis, Characterization and Biological Activity of Silver Nanoparticles Using Ruta Leaf Extract", *J. Phys.: Conf. Ser.*, 1999, 012050, (2021).
[10] M. Ndikau et al., "Green Synthesis and Characterization of Silver Nanoparticles Using Citrullus lanatus Fruit Rind Extract", *Int. J. Anal. Chem.*, 2017, Article ID 8108504.
[11] G.A. Naeem et al., "Punica granatum L. mesocarp-assisted rapid fabrication of gold nanoparticles and characterization of nano-crystals", *Enviro. Nanotechnol. Monitor. Manag.*, 14 (2020) 100390.
[12] M.N. Owaid et al., "Synthesis, Characterization and Antitumor Efficacy of Silver Nanoparticle from Agaricus bisporus Pileus, Basidiomycota", *Walailak J. Sci. Tech.*, 17(2) (2020) 75-87.
[13] S.J. Ahmed et al., "Mycosynthesizing and characterizing silver nanoparticles from the mushroom Inonotus hispidus (Hymenochaetaceae), and their antibacterial and antifungal activities", *Enviro. Nanotechnol. Monitor. Manag.*, 14 (2020) 100313.
[14] R.F. Muslim, M.M. Saleh and S.E. Saleh, "Synthesis and characterization of new sulphur six-membered heterocyclic compounds and evaluation their biological activity", *Revista Aus*, 26(2) (2019) 129-135.
[15] S.M. Roopan et al., "Low-cost and eco-friendly phyto-synthesis of silver nanoparticles using Cocos nucifera coir extract and its larvicidal activity", *Ind. Crops Prod.*, 43 (2013) 631-635.
[16] K. Anandalakshmi, J. Venugobal and V. Ramasamy, "Characterization of silver nanoparticles by green synthesis method using Pedalium murex leaf extract and their antibacterial activity", *Appl. Nanosci.*, 6 (2016) 399-408.
[17] N.M. Abd-Alghafour, I.H. Kadhim and G.A. Naeem, "UV detector characteristics of ZnO thin film depositedon Corning glass substrates using low-cost fabrication method", *J. Mater. Sci.: Materials in Electronics*, (2021).
[18] A.N. Ghassan et al., "Green Synthesis of Gold Nanoparticles from Coprinus comatus, Agaricaceae, and the Effect of Ultraviolet Irradiation on Their Characteristics", *Walailak J. Sci. Tech.*, 18(8) (2021) 9396.
[19] E. Gurgur et al., "Green synthesis of zinc oxide nanoparticles and zinc oxide–silver, zinc oxide–copper nanocomposites using Bridelia ferruginea as biotemplate", *SN Appl. Sci.*, 2 (2020) 911.
[20] E.A.M. Hussein et al., "Biologically Synthesized Silver Nanoparticles for Enhancing Tetracycline Activity Against Staphylococcus aureus and Klebsiella pneumonia", *Braz. Arch. Bio. Technol.*, 62 (2019) ??-??.
[21] S.V. Patil et al., "Biosynthesis of silver nanoparticles using latex from few euphorbian plants and their antimicrobial potential", *Appl. Biochem. Biotechnol.*, 167 (2012) 776-790, (2012).
[22] K.N. Nahar et al., "Green synthesis of silver nanoparticles from Citrus sinensis peel extract and its antibacterial potential", *Asian J. Green Chem.*, 5(1) (2021) 135.
[23] V.S. Kotakadi et al., "New generation of bactericidal silver nanoparticles against different antibiotic resistant Escherichia coli strains", *Appl. Nanosci.*, 5(7) (2015) 847-855.
[24] V.S. Kotakadi et al., "Biofabrication and spectral characterization of silver nanoparticles and their cytotoxic studies on human CD34+ve stem cells", *Biotech*, 6(2) (2016) 216.
[25] A.K. Suresh et al., "Monodispersed biocompatible silver sulfide nanoparticles: facile extracellular biosynthesis using the c-proteobacterium, Shewanella oneidensis", *Acta Biomaterialia*, 7(12) (2011) 4253-4258.

Scanning Electron Microscopy of Si-CNT Structures Used for Solar Cell Fabrication

Zahraa B. Ibraheem[1], Mohammad M. Uonis[1], Mazin A. Abed[2]

[1] Department of New and Renewable Energy, College of Science, Mosul University, Mosul, IRAQ
[2] Department of Physics, College of Science, Mosul University, Mosul, IRAQ

Abstract
Plasma sputtering technique was used to deposit carbon layers with different nano scale thicknesses on p-type silicon wafers. The scanning electron microscope images showed that the grains size grow and aggregate in a cluster. The properties of the junction gave a proof of the formation of carbon nanotubes.

Keywords: Carbon nanotubes; Solar cells; p-n junction; Cold plasma
Received: 1 April 2021; **Revised:** 5 June 2021; **Accepted:** 9 September 2021; **Published:** 1 March 2022

1. Introduction

The importance of carbon as a chemical element comes from the ability of its large atoms to bond with each other or with atoms of different chemical elements in different ways [1]. This diversity in bonding gives a diversity of structural forms, including crystalline carbon such as graphite and fullerene, amorphous carbon and carbon nanoparticles, including carbon nanotubes, each of these shapes is characterized by different properties, including a low coefficient of friction, high thermal conductivity, optical transmittance, hardness, as well as being non-toxic or harmful to the environment [2-4]. Fullerene particles have attracted great interest in recent research because of their distinct electrical and mechanical properties, including high electrical conductivity, hardness, and others. Fullerene molecules are the basis for the construction of carbon nanotubes, because the ends of the carbon nanotubes are in the form of fullerene molecules [5]. Each carbon atom in the fullerene is aligned with three other carbon atoms and the positions of the carbon atoms in the fullerene molecule (C_{60}) are identical and are located at a fixed distance from the center of the molecule (approximately 3.55Å) and the average distance between each two adjacent carbon atoms of 1.44 Å and the fullerene (C_{60}) can be counted as a coiled graphite layer that generates a symmetric polyhedral shape consisting of 20 hexagonal rings and 12 pentagonal rings needed to form curved surfaces and this agrees with Euler's theorem [6,7]. The carbon nanotubes are originally bi-directional strips of graphene wrapped around a specific axis to form a cylindrical shape with a diameter ranging between (50-0.4 nm), each carbon atom hybrid (sp^2) has three covalent bonds With three other carbon atoms, and the fourth electron is in un hybridized orbital π and since the unit cell in graphene includes two atoms, there will be even numbers of electrons that can give the conductor or semiconductor properties of carbon nanotubes [8]. Different techniques have been used in the preparation of carbon nanotube such as hot-filament (HF-CVD) [9-13], thermal chemical vapor deposition [14,15], plasma-enhanced chemical vapor deposition (PECVD) [16-18], and laser ablation technique [19,20].

In this study, different thickness of carbon nano layers (30.5, 52.6 and 70.12 nm) have been used in the preparation of Si-CNT solar cell, carbon layers were examined using scanning electron microscopy.

2. Experimental Method

Carbon nano layers have been deposited on silicon wafers to prepare Si-CNT junction using plasma sputtering technique. The impurities expected to be formed on the surface of silicon strips can be divided into

three categories, contamination fills, discreet particles and absorbed gas atoms as a result of processing silicon strips during the preparation. In the process of cleaning the silicon wafers, chemical compounds are used as solvents for removing different types of impurities, and it includes a set of successive steps in which the silicon wafers is washed with distilled water for 2-3 minutes, washed with ethanol solution by ultrasonic for a period of 5-10 minutes, washed with distilled water for 2-3 minutes, washed with ultrasonic acetone solution for 5-10 minutes, washed with distilled water for 2-3 minutes and then immersed in hydrofluoric acid (HF) at a concentration of 9% for one minute to remove a layer of silicon dioxide generated as a result of oxidation, washed with distilled water for 2-3 minutes and finally immersed in acetone solution in order for the model to be dried directly [14,15]. The plasma atomization technique was used to deposit a layer of carbon with different thicknesses (30.5, 52.6 and 70.12 nm) of pure graphite columns (99.9%) in a vacuum chamber of 10-2 mbar in an atmosphere of argon gas, the device used in the plasma atomization process is Q150R S/E/ES shown in Fig. (1).

The device-specific variables are determined by which the thickness and structure of the carbon deposited layer can be controlled according to the amount of current passing through the carbon column, the time of the pulses and the number of pulses as shown in tables (1) and (2).

Table (1) Values of variables used in carbon deposition

Parameter	Value
Material	Carbon
Pulse Current	70 A
Pulses Length	10 s
Number of Pulses	5
Out Gas Time	60 s
Out Gas Current	50 A

Table (2) Values of variables used in gold deposition

Parameter	Value
Material	Gold
Sputter Current mA	70 A
Terminate thickness (nm)	70 nm
Tooling factor	5
Out Gas Time	30 second
Out Gas Current	50 A

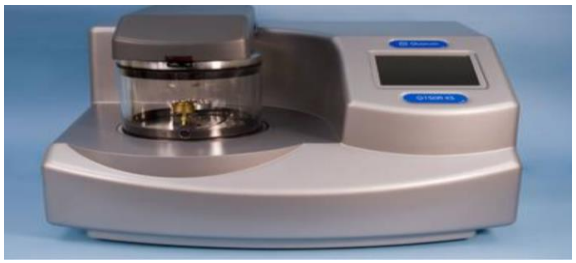

Fig. (1) Photograph of the Q150R S/E/ES plasma atomization system

3. Results and Discussion

Silicon wafers (p-type) have been used as a substrate to deposit different thickness of carbon nano layers (30.5, 52.6 and 70.12 nm) in the preparation of silicon-carbon nanotube junction (Si-CNT), carbon layers have been examined using scanning electron microscope (SEM).

Figure (2) shows the Scanning electron microscope SEM images of the carbon layers, The images showed aggregates of carbon nanoparticles, which took the form of clusters, and also showed a slight change in the size of the grains with the change in the thickness of the carbon layer, this is due to the fact that the plasma during the deposition process scrapes the carbon layer as a result of the proximity of the samples surfaces to the plasma, which will negatively affect the growth of the grains [21-23].

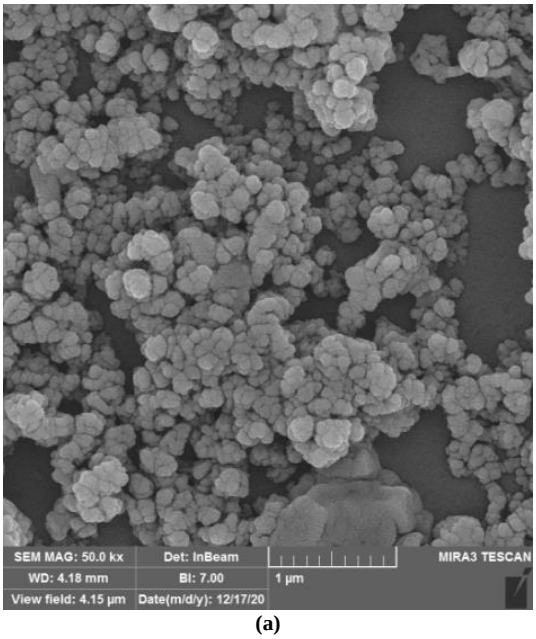

(a)

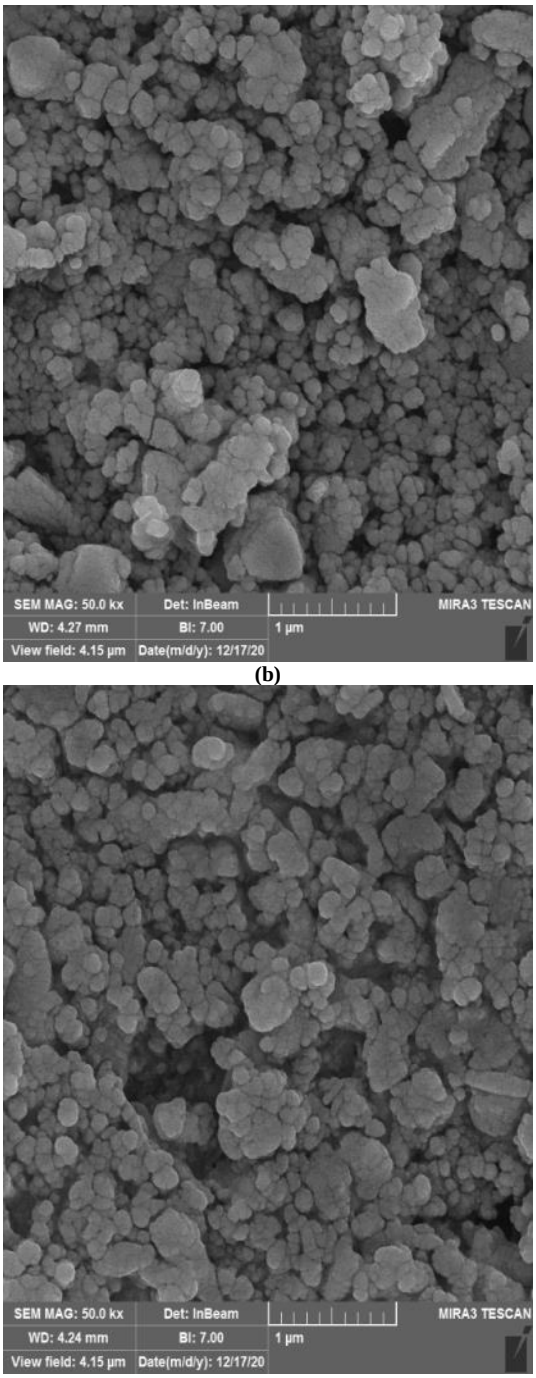

Fig. (3) SEM images of carbon layers with different thicknesses (a) 30.5 nm, (b) 52.6 nm and (c) 70.12 nm

The effect of light intensity on the out power of the Si-CNT solar cell with different concentration of carbon layer are shown in Fig. (2). The junction for all thicknesses behaves as an n-type semiconductor and this proves that the carbon nanotubes are of the multi-walled type because this type of tubes always behaves as a semiconductor [24,25]. The short circuit current and open circuit voltage increases for all thicknesses of carbon layers as a result of the increases of carbon nanotube density.

4. Conclusions

The carbon nanotubes have been constructed on a p-type silicon wafer substrates without catalysts. Scanning electron microscope showed that the grain size increases slightly with layer thickness.

References

[1] T.D. Burchell, **"Carbon Materials for Advanced Technologies"**, 1st ed., Elsevier Science, Ltd. (Oxford, 1999).

[2] A. Hirsch, "The era of carbon allotropes", *Nat. Mater.*, 9 (2010) 868-871.

[3] T. Pradeep, "Nano: the essential, understanding the nanoscience and nanotechnology", Tata McGraw-Hill Pub. Co., Ltd. (New Delhi, 2007).

[4] D.J. Hornbaker, "Electronic Structure of Carbon Nanotube Systems Measured with Scanning Tunneling Microscopy", Ph.D. thesis, University of Illinois at Urbana-Champaign (2003).

[5] E.H. Wahl, "Laser-Based Diagnostics of Diamond Synthesis Reactors", Report No. TSD-136, The U.S. Department of Energy, Basic Energy Sciences, Stanford University (2001).

[6] E.N. Ganesh, "Single Walled and Multi Walled Carbon Nanotube Structure, Synthesis and Applications", *Int. J. Innov. Technol. Explor. Eng.*, 2(4) (2013) 311-320.

[7] E.N. Farabaugh, A. Feldman and L. Robins, "Influence of Filament Geometry on Hot Filament Growth of Diamond Films", 2nd Int. Conf. on Now Diamond Sci. Technol., National Institute of Standards and Technology Ceramics Division Gathersburg, MD 20899 (1991).

[8] R.A. Ismail et al., "Characterization of Si p-n Photodetectors Produced by Laser-Induced Diffusion", *Int. J. Mod. Phys.*, 19(31) (2005) 4619-4628.

[9] O.A. Hamadi, R.A. Markub and A.A.K. Hadi, "Heat-annealed enhanced-diffusion of silver in gallium arsenide", *J. Edu. Al-Mustansiriya Univ.*, 3 (2001) 35-44.

[10] R.A. Ismail et al., "Full Characterization at 904nm of Si p-n Junction Photodetectors Produced by LID Technique", *Eur. Phys. J.: Appl. Phys.*, 38 (2007) 197-201.

[11] F. Jurg, "Growth of Single-Wall Carbon Nanotubes by Chemical Vapor Deposition for Electrical Devices", Ph.D. thesis, Universitat Basel (2006).

[12] O.A. Hamadi and K.Z. Yahiya, "Optical and electrical properties of selenium-antimony heterojunction formed on silicon substrate", *Sharjah Univ. J. Pure Appl. Sci.*, 4(2) (2007) 1-11.

[13] M. Daenen et al., "The Wondrous World of Carbon Nanotubes: a review of current carbon nanotube technologies", Phillips NAT-lab, Eindhoven University of Technology (2003).
[14] A. Szabó et al., "Synthesis Methods of Carbon Nanotubes and Related Materials", *Materials*, 3 (2010) 3092-3140.
[15] O.A. Hamadi, "Characteristics of CdO-Si Heterostructure Produced by Plasma-Induced Bonding Technique", *Proc. IMechE, Part L, J. Mater.: Design & Appl.*, 222 (2008) 65-71.
[16] T. Steiner, "Semiconductor Nanostructures for Optoelectronic Applications", Artech House, Inc. (Boston, 2004).
[17] C.D. Scott et al., "Growth mechanisms for single-wall carbon nanotubes in a laser-ablation process", *Mater. Sci. Process. Appl. Phys.*, A72 (2001) 573-580.
[18] M. Musaddique, A. Rafique and J. Iqbal, "Production of Carbon Nanotubes by Different Routes - A Review", J. Encapsul. Adsorp. Sci., 1 (2011) 29-34.
[19] O.A. Hamadi, "Effect of Annealing on the Electrical Characteristics of CdO-Si Heterostructure Produced by Plasma-Induced Bonding Technique", *Iraqi J. Appl. Phys.*, 4(3) (2008) 34-37.
[20] W. Kern, "The Evolutionof Silicon Wafer Cleaning Technology", *J. Electrochem. Soc.*, 137(6) (1990) 1887-1891.
[21] Virginia Semiconductor, Inc., **"Wet-Chemical Etching and Cleaning of Silicon"**, (2003) www.virginiasemi.com.
[22] M.M. Uonis, B.M. Mustafa and A.M. Ezzat, "The Role of Sputtering Current on the Optical and Electrical Properties of Si-C Junction", *World J. Nano Sci. Eng.*, 4 (2014) 90-96.
[23] O.A. Hamadi, "Profiling of Antimony Diffusivity in Silicon Substrates using Laser-Induced Diffusion Technique", *Iraqi J. Appl. Phys. Lett.*, 3(1) (2010) 23-26.
[24] M.M. Uonis, B.M. Mustafa and A.M. Ezzat, "The Effect of Carbon Rod-Specimens Distance on the Structural and Electrical Properties of Carbon Nanotube", *World J. Nano Sci. Eng.*, 4 (2014) 105-110
[25] M.S. Dresselhaus, G. Dresselhaus and R. Saito, "Physics of Carbon Nanotubes", *Carbon*, 33(7) (1995) 883-891.

Optical Properties of CdO Nanostructures Prepared by Plasma Jet Technique

Omar A. Gadaan[1], K. H. Razyg[1], Kadhim A. Aadim[2]

[1] Department of Physics, College of Education for Pure Sciences, Tikrit University, IRAQ
[2] Department of Physics, College of Science, University of Baghdad, Baghdad, IRAQ

Abstract
In the present study, nanoparticles of cadmium oxide have been prepared from bulk structure by the induced plasma technique at different bombardment times. These nanoparticles were prepared as thin layers on glass substrates with different thicknesses. These films were analyzed with UV-visible spectrophotometry. When the optical properties and their constants were measured, the energy gap of the films increased in the range of 2.94-3.2 eV with bombardment times.

Keywords: Plasma Jet, Optical properties; Structural properties; Energy gap; Roughness; Nano particles.
Received: 1 April 2021; **Revised:** 5 June 2021; **Accepted:** 9 September 2021; **Published:** 1 March 2022

1. Introduction

Cadmium oxide (CdO) is a semiconductor material within the group of transparent conductive oxides (TCO) and has distinct properties, including a relatively large energy gap range of 2.2-2.7 eV [1-5], transparency in the visible region Near infrared rays (NIR) [6,7], high reflectivity in the red region of the electromagnetic spectrum [8,9], high mobility of carriers [10], high electrical conductivity similar to the conductivity of negative-type metals (n-type) [11,12], and has good fluorescence, cadmium oxide has many applications such as electro-optical devices [13], phototransistors [14], biological and catalytically applications [15], and gas sensors [16]. Several techniques have been used in the preparation of cadmium oxide thin films, such as magnetron sputtering [17,18], sol gel method [19] and spray pyrolysis technique [20].

2. Preparation Method

Solutions containing nanoparticles were prepared by the induced plasma deposition method for different preparation periods (4, 6, 8 and 10 min). Cadmium metal foils 99% purity have been used as a source for cadmium. The cleaning of the foils was carried out using polishing paper and then washed with ethanol alcohol to remove any impurities present on the surface of the metals.

As the cadmium metal before placing it in the glass beaker had dimensions of length and width of about 10 cm^2, after that, a part of the cadmium metal was cut to about 1.5 cm^2, it will be immersed in a 10 ml glass beaker containing 7 ml of distilled water. The needle nozzle is directed in the middle of the metal. If a needle nozzle is located at a distance of 7 cm^2 from the target, then in order to generate a spark in the form of a scattered blue flame, the metal foil will be connected to the positive electrode while the negative electrode will be connected to the needle nozzle. The process will be carried out in the presence of argon gas that flows at a constant rate (3 L/s).

3. Results and Discussion

The cadmium oxide CdO particles have been prepared using the plasma-jet technique for different preparation periods (bombardment) in the range of 4, 6, 8, and 10 min. The optical properties of CdO particles in each solution were taken. Figures (2-6) shows the optical properties and constants for the solution that was prepared at different periods. The transmittance, absorbance, and reflectance were varied rapidly over the range of 300-400 nm and then extremely saturated for the longer wave lengths. This change also occurs similarly in the optical constants and for the same range of wavelengths, where we notice the refractive index and the extinction

coefficient decrease with wavelength in the range of 300-400nm and then become extremely constant for the other longer wavelengths.

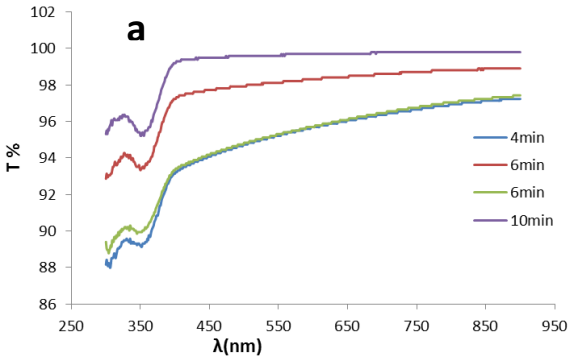

Fig. (1) Transmission spectra of the prepared thin films prepared at different bombardment times

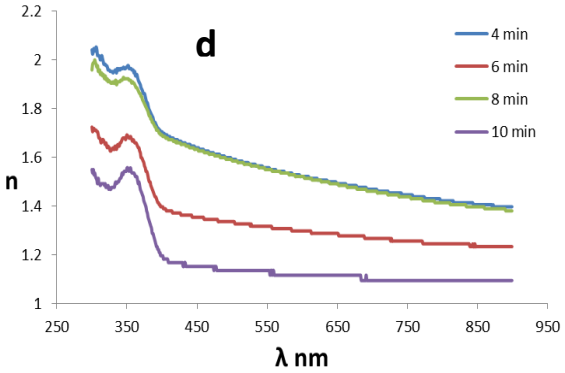

Fig. (2) Variation of refractive index with wavelength for the prepared thin films prepared at different bombardment times

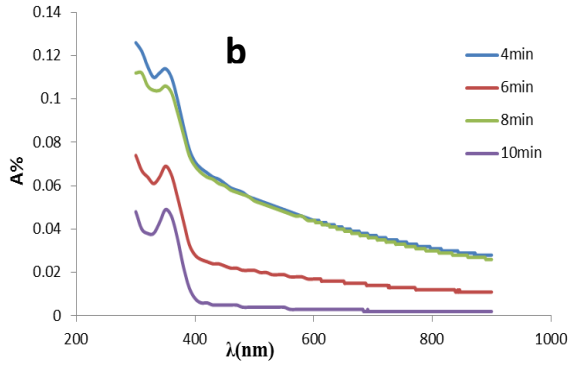

Fig. (3) Absorption spectra of the prepared thin films prepared at different bombardment times

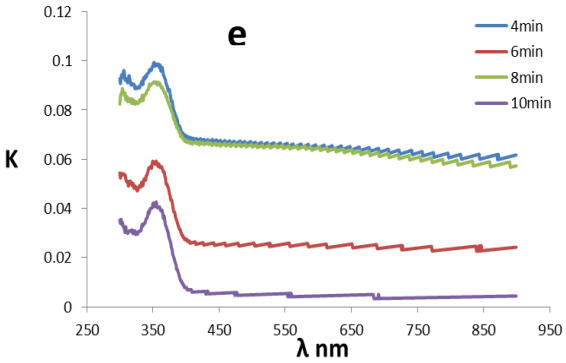

Fig. (4) Variation of extinction coefficient with wavelength for the prepared thin films prepared at different bombardment times

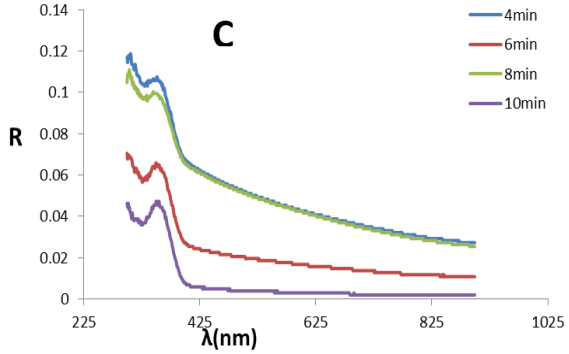

Fig. (5) Reflection spectra of the prepared thin films prepared at different bombardment times

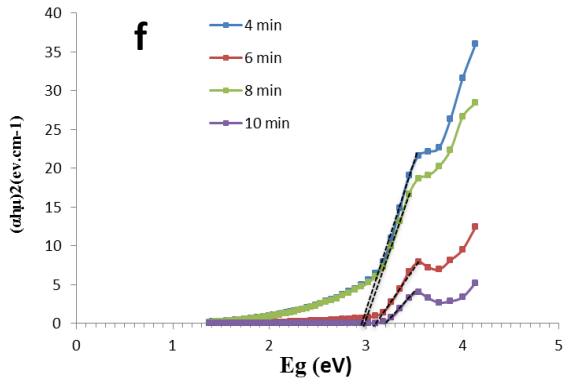

Fig. (6) Relationship of $(\alpha h\nu)^2$ with photon energy (hν) for the prepared thin films prepared at different bombardment times

The calculated band gap for all solutions changed clearly in Fig. (7). The band gap for the particles prepared at 4 min was 2.96 eV, then decreased to 2.94 eV for the particles prepared at 6 min, while it increased to 3.1 eV and 3.2 eV for the particles prepared at 8 and 10 min, respectively. The fluctuation in the band gap is due to the variation in the grain size, where we note that the energy gap increases when the grain size approaches the Nano scale.

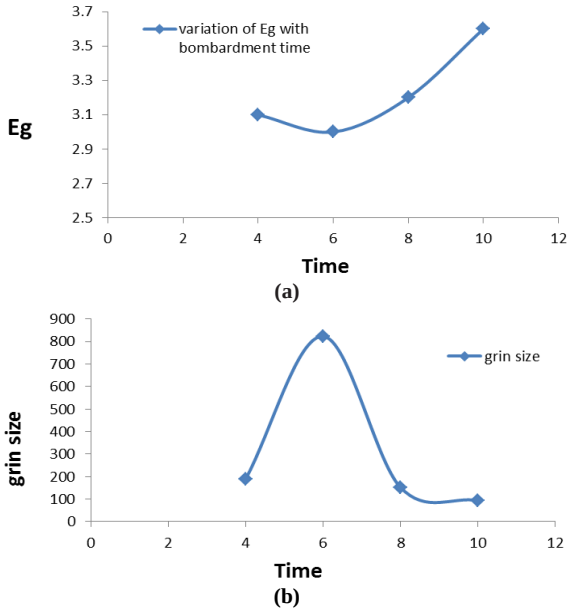

Fig. (7) (a) Variation in energy band gap (E_g) with bombardment time; (b) variation in grin size with bombardment time

4. Conclusions

Cadmium oxide nanoparticles have been prepared using the plasma-Get technique for different bombardment periods. AFM images show that the roughness and surface thickness decrease with bombardment periods, and this agrees with SEM images and the X-ray spectrum. The X-ray spectra show that the layers are completely crystalline. The peaks for all periods appear at the same 2θ with different intensities. In addition, the calculated grain size decreases with periods from 5.4 to 3.5 nm. The optical properties and energy gap varied clearly with bombardment periods.

References

[1] P. Pradyot, **"Handbook of Inorganic Chemicals"**, McGraw-Hill, Inc., (2003) 152.

[2] C.H. Bhosale et al., "Structural, optical and electrical properties of chemically sprayed CdO thin films", *Mater. Sci. Eng. B*, 122 (2005) 67–71.

[3] T. Ghoshal, S. Kar and S. Chaudhuri, "Synthesis of nano and micro crystals of $Cd(OH)_2$ and CdO in the shape of hexagonal sheets and rods", *Appl. Surf. Sci.*, 253 (2007) 7578–7584.

[4] O.A. Hamadi, "Characteristics of CdO-Si Heterostructure Produced by Plasma-Induced Bonding Technique", *Proc. IMechE, Part L, J. Mater.: Design & Appl.*, 222 (2008) 65-71.

[5] A.A. Dakhel and A.Y. Ali-Mohamed, "Structural, electrical, and optical absorption properties of $LaxCd_{1-x}O$ solid solution films obtained by sol–gel method", *Mater. Chem. Phys.*, 113 (2009) 356–360.

[6] O.A. Hamadi, "Effect of Annealing on the Electrical Characteristics of CdO-Si Heterostructure Produced by Plasma-Induced Bonding Technique", *Iraqi J. Appl. Phys.*, 4(3) (2008) 34-37.

[7] S. Ilican et al., "CdO:Al films deposited by sol–gel process: a study on their structural and optical properties", Optoelectron. Adv. Mater. – Rap. Commun., 3(2) (2009) 135-140.

[8] D.M. Carballeda-Galicia et al., "High transmittance CdO thin films obtained by the sol-gel method", Thin Solid Films, 371(1-2) (2000) 105-108.

[9] O.A. Hamadi, N.J. Shakir and F.H. Mohammed, "Magnetic Field and Temperature Dependent Measurements of Hall Coefficient in Thermal Evaporated Tin-Doped Cadmium Oxide Thin Films", *Bulg. J. Phys.*, 37(4) (2010) 223-231.

[10] Y. Caglar, S. Ilican and M. Caglar, "Single-oscillator model and determination of optical constants of spray pyrolyzed amorphous SnO_2 thin films", *Eur. Phys. B*, 58(3) (2007) 251-256.

[11] A.A. Dakhel, "Influence of hydrogenation on the electrical and optical properties of CdO:Tl thin films", *Thin Solid Films*, 517 (2008) 886–890.

[12] A. Badawi et al., "Tailoring the optical properties of CdO nanostructures via barium doping for optical windows applications", *Phys. Lett. A*, 411 (2021).

[13] Y. Zhang and J. Mu, "Preparation of CdO Thin Films by Annealing Cd^{+2}-Dithiol Self-Assembled Films", Disper. Sci. Technol., 26 (2005) 509–511.

[14] M. Uonis, B. Mustafa and A. Ezzat, "The Role of Sputtering Current on the Optical and Electrical Properties of Si-C Junction", *World J. Nano Sci. Eng.*, 4 (2014) 90-96.

[15] Oday A. Hammadi, "Magnetically-Supported Electrically-Induced Formation of Silicon Carbide Nanostructures on Silicon Substrate for Optoelectronics Applications", *Opt. Quantum Electron.*, 54(7) (2022) 427.

[16] X. Li et al., "High Mobility CdO Films and Their Dependence on Structure", *Electrochem. Solid State Lett.*, 4 (2001) 66-68.

[17] A.A. Dakhel and A.Y. Ali-Mohamed, "Structural and optoelectrical properties of nanocrystalline Gd-doped CdO films prepared by sol-gel method", *Sol-Gel Sci. Technol.*, 55 (2010) 348–353.

[18] R.K. Gupta et al., "Wide band gap $Cd_{0.83}Mg_{0.15}Al_{0.02}O$ thin films by pulsed laser deposition", *Appl. Surf. Sci.*, 255 (2009) 4466-4469.

[19] Z. Zhao et al., "Electrical and optical properties of tin-doped CdO films deposited by atmospheric metalorganic chemical vapor deposition", *Thin Solid Films*, 413 (2002) 203-211.

[20] S.M. Sze, **"Physics of Semiconductor Devices"**, John Wiley and Sons (NY, 1986).

[21] K.H. Mahmoud, Z.M. El–Bahy and A.I. Hanafy, "Photoluminescence analysis of Er nanoparticles in cadmium–phosphate glasses", *J. Non–Cryst. Solids,* 363 (2013) 116–120.

[22] A.M. Mostafa et al., "Synthesis of Cadmium oxide Nanoparticles by Pulsed laser ablation in liquid environment", *Int. J. Light Electron Opt.*, 144 (2017) 679-684.

[23] N.A.H. Hashim and F.J. Kadhim, "Structural and Optical Characteristics of Co3O4 Nanostructures Prepared by DC Reactive Magnetron Sputtering", *Iraqi J. Appl. Phys.*, 18(4) (2022) 31-36.

[24] B. Goswami and A. Choudhury, "Enhanced visible luminescence and modification in morphological properties of Cadmium oxide Nanoparticles induced by annealing", *J. Exp. Nanosci.*, 10(12) (2014) 900-910.

[25] K. Viswanathan and F.C. Bor, "Synthesis and characterization of poly(N–vinylpyrrolidine)–silica hybrid shell coated cadmium selenide/cadmium sulphide and cadmium selenide/zinc sulfide nanoparticles", *Mater. Lett.*, 65(4) (2011) 646–649.

Optical Properties of Nanostructured Nickel Oxide Thin Films Prepared by Induced Plasma Technique

Omar A. AL Rhhauy[1], K.H. Razyg[2], Kadhim A. Aadim[3]

[1] Department of Physics, College of Education for Pure Sciences, Tikrit University, IRAQ
[2] Department of Physics, College of Science, University of Baghdad, Baghdad, IRAQ

Abstract
In the current study, nickel oxide nanoparticles were made from bulk structure using the induced plasma process and various bombardment periods. These nanoparticles were created as thin layers on various thicknesses of glass substrates (prepared at different times of shelling). After that, they were analyzed with an x-ray spectrum, scanning electron microscope, atomic force microscope, and UV-visible spectrophotometer. When the optical constants and characteristics were measured, the films' energy gaps ranged from 1.85 eV to 2.1 eV depending on the bombardment periods. The AFM and SEM examination tools clearly reveal a structural change where the roughness varies with bombardment time due to the variation in the diameter of the nanoparticles. Finally, layers are completely crystalline by the x-ray spectrum.

Keywords: Induced plasma; Optical properties; Structure properties; Energy gap; Roughness
Received: 1 April 2021; **Revised:** 5 June 2021; **Accepted:** 9 September 2021; **Published:** 1 March 2022

1. Introduction

Nickel is a chemical element with atomic number 28, a shiny silver-white metal with a touch of gold. Nickel is a transition metal hard and malleable [1-3]. However, only small amounts of nickel are found in the atmosphere [4]. Within large nickel-iron meteorites that are not exposed to oxygen outside the Earth's atmosphere [5]. It is believed that a mixture of iron and nickel forms the outer shell of the planet [6,7]. Nickel has many uses, especially in alloys. This includes the rapidly growing battery industry as a vehicle for electric vehicles [8]. Nickel has many special uses in chemical manufacturing, such as hydrogenation catalysts, battery cathodes, dyes, and metal surface treatments [9]. Nickel is an essential nutrient for some microorganisms and plants that contain enzymes that use nickel as their active site [10].

Nickel is found in meteorites and can usually be found only in small quantities, but the largest source of it is in some ores, the minerals composed of iron, copper, and nickel [11]. Perhaps this raw material is the most abundant source, since it is extracted and sent to most of the industrial regions of the world [12]. As for how to extract it, the nickel-bearing ore is smelted in a high-temperature furnace, resulting in a fertile mixture or mixture of metals [13]. This mixture turns into nickel by mixing it with coke and heating it in an oven at a high temperature [14]. Nickel is known for its shiny silver color and density, which is hard and malleable under heat [15]. This means that it can be modified in the desired way and shape.

2. Process of Preparation

Using the induced plasma deposition approach, solutions containing nanoparticles were created for various preparation times 4, 6, 8 and 10 min. The nanoscale nickel has been obtained from 99% pure metal foils. The foils were cleaned with polishing paper and then washed with ethanol alcohol to get rid of any impurities on the metal's surface. Where the Ni metal before placing it in the glass beaker had dimensions of length and width of about 5 cm^2, after that, a part of the Ni metal was cut to about 1.5 cm^2. It will be submerged in a 10 ml beaker with 7 ml of distilled water, where the nozzle of the needle is directed in the middle of the metal. The metal foil will be linked to the positive electrode, while the negative electrode will be connected to the needle nozzle. If a needle nozzle is 7 cm from the target in order to produce a spark in the shape of a scattered blue flame. The process

was carried out in the presence of argon gas that flows at a constant rate (3 L/s).

3. Results and Discussion

The induced plasma technique has been used to bombardment the nickel oxide particles for varying preparation times (bombardment) ranging at 4, 6, 8 and 10 min. Each solution's NiO particles' optical characteristics were recorded. The optical characteristics and constants for the solution created at various times are shown in Fig. (1). Over the wavelength range of 300–400 nm, the transmittance, absorbance, and reflectance rapidly changed before becoming extremely saturated for the longer wave lengths. The refractive index and the extinction coefficient both decline with wavelength in the range of 300–400 nm and then become remarkably stable for the other longer wavelengths. This change also occurs similarly in the optical constants for the same wavelength range.

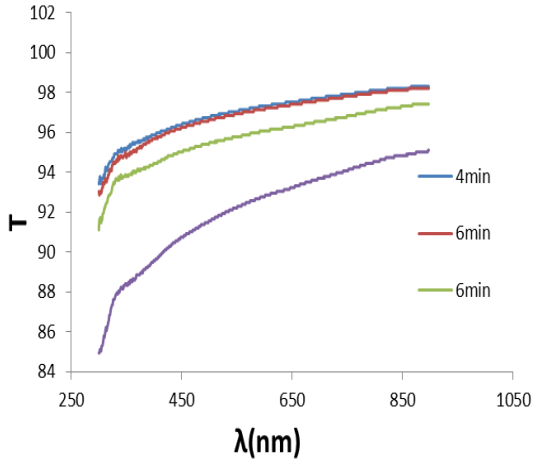

(a)

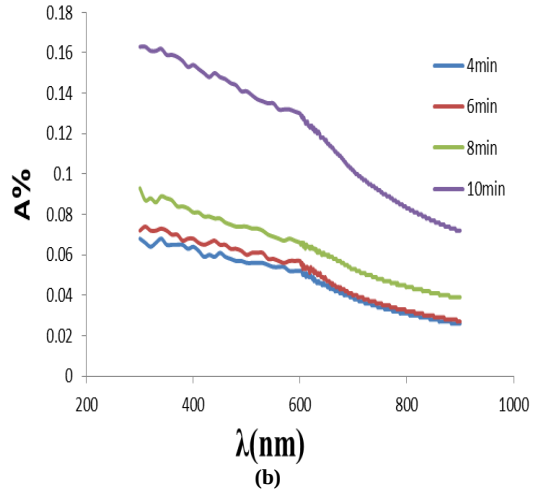

(b)

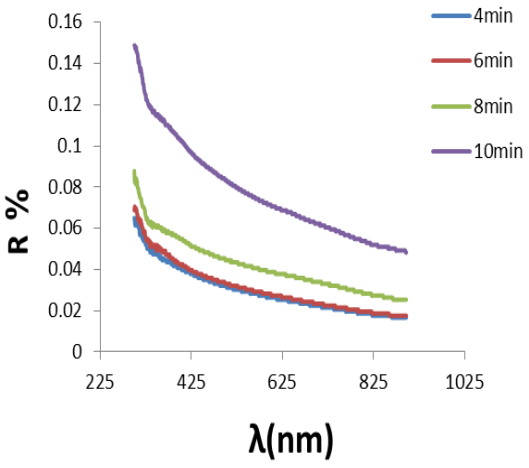

(c)

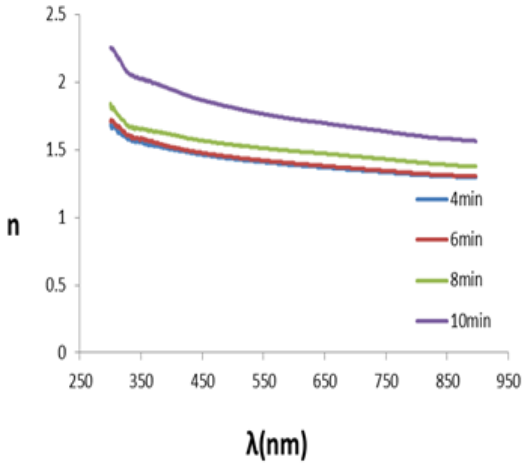

(d)

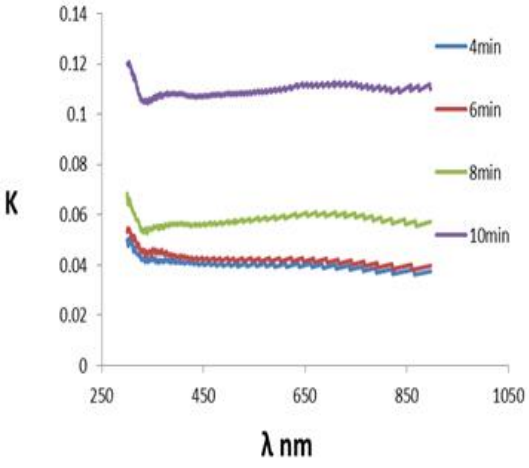

(e)

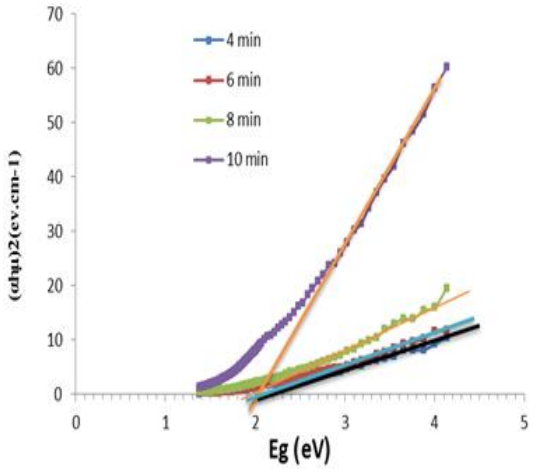

(f)

Fig. (1) Effect of bombardment time on the optical properties (a) transition, (b) absorption, (c) reflective, (d) refractive index, (e) extinction coefficient, and (f) energy gap

For each option, the predicted band gap in Fig. (2) altered significantly. The energy band gap was 2 eV for the particles prepared at 4 min, 1.85 eV at 6 min, and subsequently increased to 1.88 eV and 2.1 eV for the particles prepared at 8 and 10 min, respectively. Figure (2a). The variation in particle size is what causes the band gap to fluctuate (Fig. 2b). We can see that the energy gap widens as the grain size gets closer to the nanoscale. Table (1) shows the change of the energy band gap with time.

Table (1) Energy band gap of the CdO prepared at different bombardment times

Bombardment time (min)	Energy gap (eV)
4	2
6	1.85
8	1.88
10	2.1

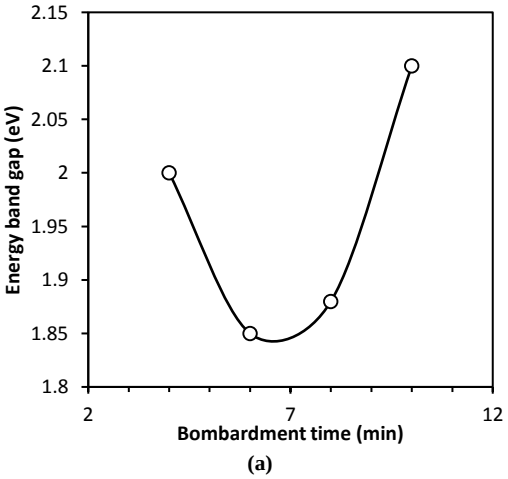

(a)

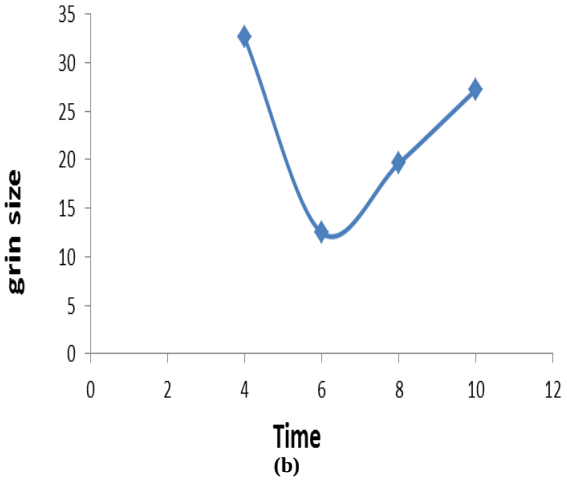

(b)

Fig. (2) (a) Variation of E_g with bombardment time, (b) Variation of grin size with bombardment time

An ionized gas called plasma has roughly equal amounts of positively and negatively charged ions and electrons [9]. Neutral atoms may be present in plasma. The plasma is referred to as partially or insufficiently ionized in this situation. If not, the plasma is referred to as totally or completely ionized [10]. The total number of positively and negatively charged particles in a partially or completely charged plasma must be balanced in order for the plasma to remain in a neutral state. The behavior and utility of plasma are frequently determined by interactions between the charged particles and the neutral particles. A plasma can have a wide range of properties depending on the type of atoms present, the ratio of ionized to neutral particles, and the energy of the particles [11].

4. Conclusions

Cadmium oxide nanoparticles have been prepared using the plasma jet technique for different bombardment periods. The optical properties and energy gap varied clearly with bombardment periods.

References

[1] Nickel: Nickel Metal Information and Data". Mindat.org . Archived from the original on March 3, 2016. Retrieved March 3, 2016. Retrieved March 2, 2016

[2] Sticksrud, Lars; Wasserman, Yevgeny; Cohen, Ronald (November 1997). Composition and temperature of the Earth's inner core. Journal of Geophysical Research. 102 (B11): 24729 - 24740. Bibcode: 1997JGR... 10224729S.

[3] O.A. Hammadi, M.K. Khalaf and F.J. Kadhim, “Fabrication of UV Photodetector from Nickel Oxide Nanoparticles Deposited on Silicon Substrate by Closed-Field Unbalanced Dual Magnetron Sputtering Techniques”, *Opt. Quantum Electron.*, 47(12) (2015) 3805-3813.

[4] Coy, J. M.D.; Skomerev, F.; Gallagher, K.; (1999). "Rare Earth Metals: Is Gadolinium Really Magnetic?". nature . 401 (6748): 35-36. Bibcode: 1999Natur.401...35C.

[5] Nickel use in society". Nickel Institute. Archived from the original on September 21, 2017

[6] R.H. Turki and M.A. Hameed, “Spectral and Electrical Characteristics of Nanostructured NiO/TiO2 Heterojunction Fabricated by DC Reactive Magnetron Sputtering”, *Iraqi J. Appl. Phys.*, 16(3) (2020) 39-42.

[7] O.A. Hammadi and N.E. Naji, “Fabrication and Characterization of Polycrystalline Nickel Cobaltite Nanostructures Prepared by Plasma Sputtering as Gas Sensor”, *Phot. Sen.*, 8(1) (2018) 43-47.

[8] M.A. Hameed, S.H. Faisal, R.H. Turki, “Characterization of Multilayer Highly-Pure Metal Oxide Structures Prepared by DC Reactive Magnetron Sputtering Technique”, *Iraqi J. Appl. Phys.*, 16(4) (2020) 25-30

[9] Treadgold, Tim. "Gold is hot but nickel is even hotter as demand for batteries in electric vehicles increases". Forbes. Retrieved October 14, 2020.

[10] Asraa M. Hameed and Mohammed A. Hameed, “Highly-Pure Nanostructured Metal Oxide Multilayer Structure Prepared by DC Reactive Magnetron Sputtering Technique”, *Iraqi J. Appl. Phys.*, 18(4) (2022) 9-14.

[11] Liu, P., Chen, D., Wang, Q., Xu, P., Long, M., & Duan, H. (2019). Crystal structure and mechanical properties of nickel–cobalt alloys with different compositions: A first-principles study. Journal of Physics and Chemistry of Solids, 109194.

[12] Asraa M. Hameed and Mohammed A. Hameed, “Spectroscopic characteristics of highly pure metal oxide nanostructures prepared by DC reactive magnetron sputtering technique”, *Emerg. Mater.*, (2022)

[13] N . Braithwaite, “Introduction to gas discharges” Plasma Sources Sci. Technol. 9 517–527,(2000).

[14] J. Diedrich," Laser-Induced Breakdown Spectroscopy on Bacterial Samples", M.Sc. thesis, Wayne State University USA, (2007).

[15] K.H. Spatschek, "Introduction to Theoretical Plasma Physics", lecture series, (2008).

Studying Effect of Laser Energy on Nickel Plasma Spectrum by Laser Induce Breakdown Spectroscopy

Huda H. Abbas, Sabah N. Mazhir

Department of Physics, College of Science for Women, University of Baghdad, Baghdad, IRAQ

Abstract
In this research, the optical emission spectrometry (OES) technique was used to study the spectrum of plasma generated from a nickel target irradiated in the air with pulses from a Q-switched Nd:YAG laser. This laser has wavelength of 1064nm, pulse duration of 10ns, repetition rate of 6Hz and energy of 300-500mJ. Plasma parameters such as electron temperature, electron density, Debye sphere length, and plasma frequency were determined using the Boltzmann-Plot and Stark broadening method. The results showed that the values of these parameters increased with increasing laser energy and the electron temperature was ranging through 0.934-1.479eV.

Keywords: Optical Emission Spectrometry technique (OES), Ni, LIBS.
Received: 1 April 2021; **Revised:** 5 June 2021; **Accepted:** 9 September 2021; **Published:** 1 March 2022

1. Introduction

The term "laser-induced plasma spectroscopy" refers to an atomic emission spectroscopy method that makes use of high-energy laser pulses to excite optical materials (LIPS) [1]. Highly purified metal spectra may be obtained by irradiating metal surfaces with high-intensity laser pulses, which produce plasma in the process [2]. Optical sample excitation is achieved by focusing a high-energy laser pulse on a small area of the sample surface [3]. To make a laser-induced plasma (LIP), the sample is first heated, then evaporated, atomized, and finally deionized in a very tiny quantity; this is a source of highly pure metal spectrum. For example, plasma light emissions may represent "spectral signatures" of many types of solid, liquid, and gaseous materials. When it comes to quick, low-precision, and low-cost chemistry analysis, LIBS is an excellent choice. Since no sample preparation is required, this method may be considered a "plug and play" method that could be used in many different situations [4-6]. High-power laser interactions with the matter may result in the formation of a transitory plasma. As a result of these factors, the repeatability of the LIBS signal is low, which is one of the key challenges that plague the deployment of LIBS technology [7-9]. The study of hardware improvement, as well as research into the system through experiment equipment, measurement environment, optimizing target material properties, and other methods of improving the accuracy of experimental data has been conducted to overcome matrix effects and improve the accuracy of experimental data [10]. It has thus become a significant research trend to increase the dependability and stability of LIBS technology by improving the spectrum of data processing, as a result of these considerations [11,12].

The purpose of this research is to evaluate the effects of laser energy on plasma emissions as well as the characterization of Ni plasmas in air.

2. Experimental LIBS Setup

Figure (1) shows a schematic diagram of the experimental setup in this work. It depicts a schematic of the LIBS experimental setup. The tests were carried out at room temperature and pressure. Nickle samples were chosen for plasma production, and the goal purity was nearly 99.9999 percent. With a Q-switched nanosecond laser source, which has an essential wavelength of 1064 nm, a pulse duration of 10 ns, and a repeating frequency of 6 Hz, the plasma was generated. Analysis of the spectrometer's optical emission was done. The distance from the spectrometer to

the laser target is around 30 cm. The laser-induced plasma light emissions from the Ni target surface were captured using an optical fiber with a 50 μm diameter core that was positioned at a 1 cm distance. NIST database software [13] was used to calibrate the optical emission line to specified elements to determine the plasma properties.

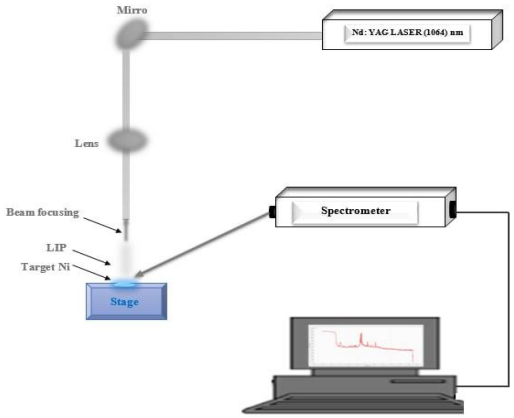

Fig. (1) Schematic diagram of the experimental setup for LIBS

3. Results and Discussion

As a result of advancements in the iterative Boltzmann technique, it is now possible to measure the electron temperature of laser coin-induced plasma. Because of the correlation coefficient of linear fitting of 0.6529 and the Boltzmann diagram of the nickel atom line, the electron temperature of the plasma in Ni is determined to be 10829.07K. The linear correlation coefficient of the line hits 0.8356 after 600 mJ laser energy of the Boltzmann method. In other words, based on the slope found above, the electron temperature of the Ni plasma is 15993.29K. Ni plasma's electrical temperature remains constant between 15993.29 and 10829.07K throughout experimentation, increasing the linear fitting coefficient (Fig. 2a and 2b) from 0.6529 to 0.8356.

Density of electrons in a laser-induced nickel plasma. Stark broadening is the primary method by which the atomic emission line broadens in a laser-induced plasma. This widening is driven by the surrounding charged particle field. The following equations [14-16] describe the connection between plasma electron density and the Stark broadening breadth [17]

$$\Delta\lambda_{1/2} = 2\omega\left(\frac{N_e}{10^{16}}\right) + 3.5\,A\left(\frac{N_e}{10^{16}}\right)^{1/4} \times \left[1 - \frac{3}{4}N_D^{-\frac{1}{3}}\right]\omega\left(\frac{N_2}{10^{16}}\right) \quad (1)$$

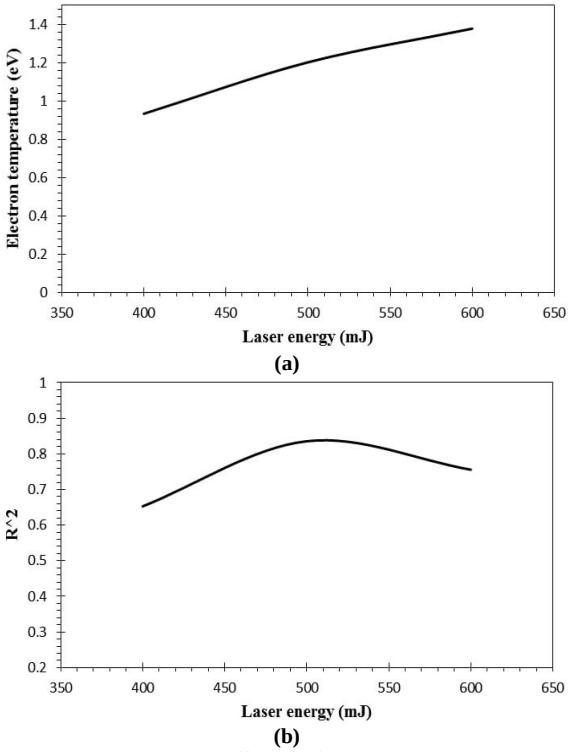

Fig. (2) (a) Correlation coefficient of laser-induced nickel plasma with laser energy, and (b) Correlation between the laser energy and the electron temperature of Ni plasma generated by LIBS

The contribution of electron widening is represented by the first item on the right in Eq. (1), while the contribution of ion broadening is represented by the second. $\Delta\lambda_{1/2}$ is Stark broadening the half peak width, ω is electron collision broadening coefficient, N_e is the number of electrons in the plasma, and N_D is the number of particles in the Debye ball, which may be represented as [18]:

$$N_D = 1.72 \times 10^9 \frac{T^{\frac{3}{2}}(eV)}{N_e^{\frac{1}{2}}(cm^{-3})} \quad (2)$$

The widening of the ionic quasi-static coulomb field is a disruption in the laser-produced plasma, according to the Stark extension theory. Because the influence of electrons on radiation atoms is so important, the ion collision broadening may be neglected in the actual computation, ignoring the second item in Eq. (1). As a result, in Eq. (1), the

connection between Stark widening the half peak width and the number of plasma electrons may be simplified as follows [19]. Table (1) lists plasma parameters of the Ni lines with different laser energy.

$$\Delta\lambda_{1/2} = 2\,\omega\,\left(\frac{N_e}{10^{16}}\right) \qquad (3)$$

The Lorentz type Stark broadening spectral line has the following function expression [20].

$$y = y_0 + \frac{2B}{\pi}\,\frac{\omega}{4\,(x-x_c)^2+\omega^2} \qquad (4)$$

where B is the spectral line's integral strength, is the whole width of the spectral line, x_c is the spectral line's center wavelength, and y_0 is the spectral line's background radiation intensity

Table (1) Plasma parameters of Ni with different laser energy

Laser energy (mJ)	slope	R^2	T_e (eV)	n_e $\times10^{18}$ (cm^{-3})	λ_D $\times10^{-6}$ (cm)	f_p $\times10^{13}$ (Hz)
400	**-1.05**	**0.65**	**0.934**	**3.030**	**4.124**	**1.563**
500	-1.11	0.83	1.203	3.210	4.549	1.609
600	**-1.15**	**0.755**	**1.379**	**3.500**	**4.663**	**1.680**

Figure (3) depicts the Stark broadening of Ni I 651.48 nm; the actual line is the Lorentz fitting curve, the square value of the correlation coefficient (R^2) is 0.83, and the spectral line's half-peak width is 0.35 nm. The plasma electron density of a Ni is 3.5 x $10^{18}cm^{-3}$, according to the Stark broadening hypothesis, which ignores other broadening effects and deducts widening instrument situations by the relevant electron collision broadening coefficient [17].

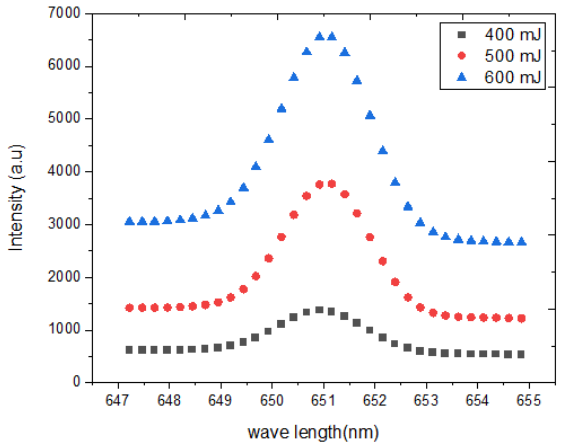

Fig. (3) Stark broadening of Ni I (651.48nm) and Lorentz fitting

Figure (4) shows the variation of electron temperature and density in a laser-induced nickel plasma as a function of laser energy, the increase of plasma temperature may be due to the plasma becomes opaque to the laser beam that reaches the target, plasma shielding occurs when the plasma reduces the transmission of laser peak energy along the beam path.

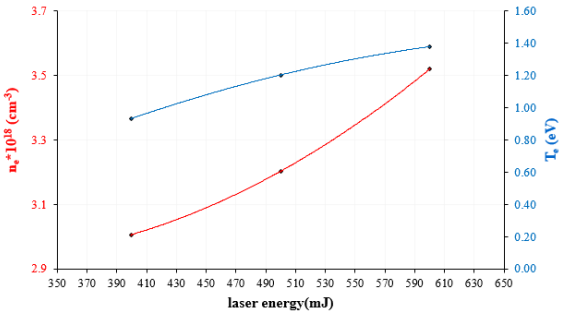

Fig. (4) Variation of electron density of laser-induced nickel plasma and electron temperature with the laser energy

4. Conclusion

The irradiance of the laser was used to model the plasma and estimate its characteristics. The higher the power of the laser, the higher the temperature of the electrons and the higher the density of the electrons. In addition to this, the plasma frequency, Debye length, and number all rose as the laser light strength increased. The findings also shown that the plasma is heated to a greater degree whenever there is interaction between the laser and the plasma.

References

[1] M. Burger, M. Skočić and S. Bukvić, "Study of self-absorption in laser induced breakdown spectroscopy", *Spectrochimica Acta Part B: Atom. Spectro.*, 101 (2014) 51-56.

[2] D.A. Cremers and L.J. Radziemski, **"Handbook of Laser-Induced Breakdown Spectroscopy"**, *John Wiley & Sons, Ltd.* (Chichester, 2006).

[3] M.L. Najarian and R.C. Chinni, "Temperature and Electron Density Determination on Laser-Induced Breakdown Spectroscopy (LIBS) Plasmas", *A Phys. Chem. Exp., J. Chem. Educ.*, 90(2) (2013) 244–247.

[4] S.A.M. Mansour, "Self-absorption effects on electron temperature-measurements utilizing laser induced breakdown spectroscopy (LIBS) techniques", *Opt. Photon. J.*, 5 (2015) 79-90.

[5] A.S. Al-Aamer and A.M. El-Sherbini, "Measurement of Plasma Parameters in Laser-Induced Breakdown Spectroscopy Using Si-Lines", *WJNSE*, 2(4) (2012) 206-212.

[6] H.A. Yuan et al., "Investigation of laser-induced plasma at varying pressure and laser focusing", *Spectrochimica Acta, Part B Atom. Spectro*., 150 (2018) 33-37.
[7] S. Hafeez, N.M. Shaikh and B. Rashid, "Plasma properties of laser-ablated strontium target", *J. Appl. Phys.*, 103(8) (2008) 083117(1-8).
[8] K.A. Yahya and B.F. Rasheed, "Effects of Discharge Current and Target Thickness in Dc - Magnetron Sputtering on Grain Size of Copper Deposited Samples", *Baghdad Sci. J*., 16(1) (2019) 84-87.
[9] S. N. Mazhir et al., "Effects of Gas Flow on Spectral Properties of Plasma Jet Induced by Microwave", *Baghdad Sci. J.*, 15(1) (2018) 81-86.
[10] N. Naeema, A. Kudher and G. Mohammed, "Study of the Spectroscopic Performance of Laser Produced CdTe, and CdTe:Ag Plasma', *IOP Conf. Ser.: Mater. Sci. Eng*., 757 (2020) 012025.
[11] N.K. Abdalameer and S.N. Mazhir, "Laser-Induced Plasma Atomic and Ionic Emission during Target Ablation", *Int. J. Nanosci.*, 20(5) (2021) 1–8.
[12] K. Rifai et al., "Quantification of copper, nickel and other elements in copper-nickel ore samples using laser-induced breakdown spectroscopy", *Spectrochimica Acta B: Atom. Spectro.*, 165 (2020) 105766.
[13] National Institute of Standards and Technology. *Atomic spectra database* [DB/OL] (2017).
[14] S.N. Mazhir et al., "A Study of Plasma parameters in gold sputtering System by Means of Optical Emission Spectroscopy", *IOP Conf. Series: Mater. Sci. Eng.*, 871 (2020) 012081.
[15] K.A. Aadim et al., "Influence of Gas Flow Rate on Plasma Parameters Produced by a Plasma Jet and its Spectroscopic Diagnosis Using the OES Technique", *IOP Conf. Ser.: Mater. Sci. Eng*., 987 (2020) 012020.
[16] S.A.M. Mansour, "Self-Absorption Effects on Electron Temperature-Measurements Utilizing Laser Induced Breakdown Spectroscopy (LIBS)-Techniques", *Opt. Photon. J.*, 5 (2015) 79-90.
[17] M. Fikry, W. Tawfk and M. Omar, "Investigation on the effects of laser parameters on the plasma profle of copper using picosecond laser induced plasma spectroscopy", *Opt. Quantum Electron*., 52 (2020) 249.
[18] W.L. Wiese, J.R. Fuhr and A. Lesage, "Experimental Stark Widths and Shifts for Spectral Lines of Neutral and Ionized Atoms (A Critical Review of Selected Data for the Period 1989 through 2000)", *J. Phys. Chem. Ref. Data*, 31(3) (2002) 819-927.
[19] A.S. Altowyan et al., "Influence of the laser wavelength on the self-absorption of Cu and Ni spectral lines by using LIBS technique", *Opt. Mater.*, 131 (2022) 112731.
[20] J. Li et al., "In-situ probing the near-surface structural thermal stability of high-nickel layered cathode materials", *Energy Storage Mater.*, 46 (2022) 90-99.

Optical Properties of New Immersion Magnetic Lens

R.Y.J. AL-Salih, Othman M.A. AL-Bayati

Department of physics, College of Sciences, University of Tikrit, Salahaddin, IRAQ

Abstract

New design of an objective magnetic immersion lens has been studied, where three innovative designs of immersion lenses were developed in a variable manner in the geometric dimensions. The axial magnetic field of these lenses was calculated by the Finite Element Method and using computer programs to study the focal properties of these lenses. L1, L2, L3 and it was found that the L3 lens achieved the best results because it had the lowest values of focal length, which corresponds to the highest values of the magnetic field, and had the lowest values of spherical aberration coefficients Cs and chromaticity Cc at a constant value of the irritant factor (NI=4800 (A-t).

Keywords: Magnetic lens; Immersion lens; Magnetic properties; Optical properties; Electronic optics
Received: 1 April 2021; **Revised:** 5 June 2021; **Accepted:** 9 September 2021; **Published:** 1 March 2022

1. Introduction

The distribution of the axial magnetic flux density and the path of the magnetic flux lines inside those lenses were studied, as well as the objective and projective optical properties of those lenses were calculated, and it was concluded that the round magnetic lens produces a relatively high peak value for the distribution of the axial magnetic flux density and the paths of the regular magnetic flux lines. Moreover, it has relatively low objective focal characteristics of focal length, spherical and chromatic aberration. This type of lens can be used as an objective lens in transmission electron microscopy [4]. In 2021, Basma and Ahmed were able to design magnetic lenses with optimal operating conditions, as they presented a study on the effect of the diameter of the axial aperture and the air gap between the poles, as well as the thickness of the pole face on the magnetic and optical properties, and they found that the optical properties and the distribution of magnetic flux density improve with Reducing the diameter of the axial aperture as well as reducing the air gap between the poles of the symmetric monopolar magnetic lens. As for the thickness of the electrode face, they found that the best magnetic properties, the highest value of magnetic flux, the lowest value of the axial magnetic field strength, and the narrowest bandwidth was when the thickness of the electrode face was equal to (4.3 mm) for the proposed design [5]. In 2021, Mardeen and Al-Jubouri studied the design of a immersed magnetic lens and it was found that the distance between the poles has a direct effect on the focal properties and found that the best distance between the poles is (2 mm) because they have the lowest values of focal length and beam diameter, which corresponds to the highest analysis value.

3. Experimental Part

The design of magnetic lenses requires determining the best geometric shape. Three models of the immersion magnetic lens were proposed, and then they were designed and named with the symbols L1, L2, L3, respectively.

The efficiency of the magnetic lens is determined by its optical properties represented by the chromatic aberration coefficient Cc and spherical Cs and the focal length $F_{\circ}$, where the chromatic aberration represents the ability of the lens to focus the electronic beam at uniform wavelengths, while the spherical aberration represents the ability of the lens to produce an electronic beam prepared in a point and less distortion, while the The focal length is the ability of the lens to focus the electronic beam [12]. And using the (MELOP) program [13]. The optical properties were calculated as a function of acceleration voltage (Vr) and as a function of the irritant factor (NI) for the three designs.

Figures (1-4) show the relationship between spherical and chromatic aberration coefficients, respectively, for lenses designed as a function of NI/SQRT (VR) irritant factor.

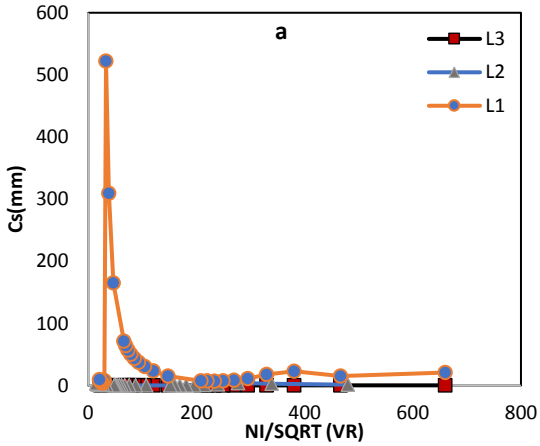

Fig. (1) Variation of spherical aberration Cs as a function of NI/SQRT irritant factor (VR) for lenses at a constant acceleration voltage Vr=10kV, (a) for the three lenses L1, L2, and L3

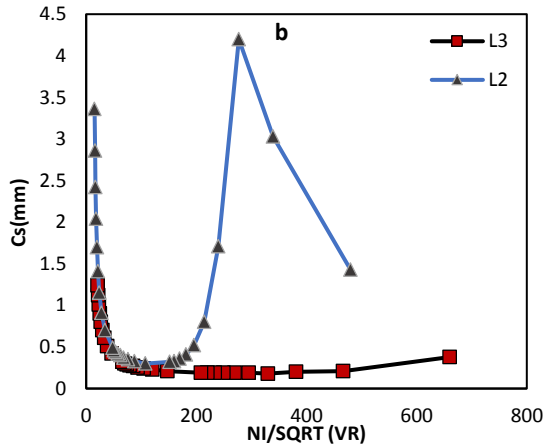

Fig. (2) Variation of spherical aberration Cs as a function of NI/SQRT irritant factor (VR) for lenses at a constant acceleration voltage Vr=10kV, (b) for the two lenses L2, L3

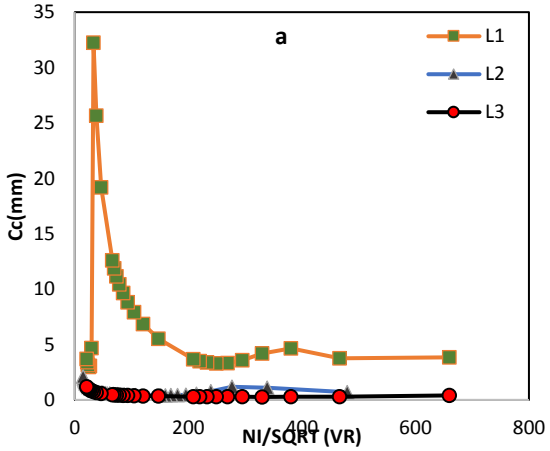

Fig. (3) Chromatic aberration change as a function of the NI/SQRT irritant factor (VR) for lenses at a constant acceleration voltage V_r=10kV, for the three lenses L1, L2, and L3

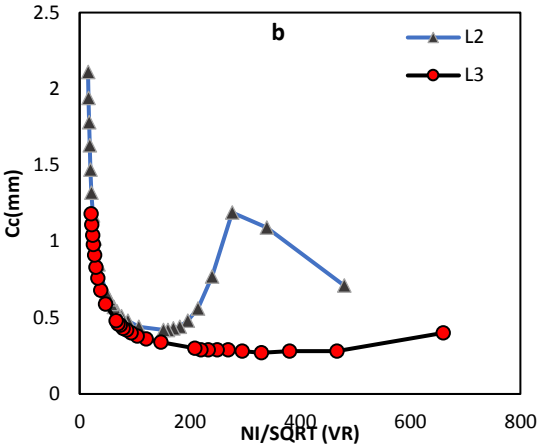

Fig. (4) Chromatic aberration change as a function of the NI/SQRT irritant factor (VR) for lenses at a constant acceleration voltage V_r=10kV, (b) for the two lenses L2, and L3

From the last two figures, the figure was divided into a and b for magnification and clarification. The difference between the lenses was found that the best uniform behavior obtained was for the L3 lens, which gave the least aberration rate. In addition, a detailed study was conducted for the focal length of the proposed lenses, and figures (5) and (6) show the comparison between the focal length as a function of the NI/SQRT irritant factor (VR) for lenses at a constant acceleration voltage Vr=10 kV.

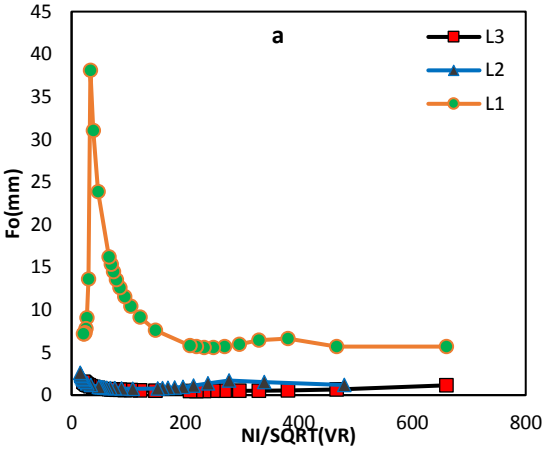

Fig. (5) Variation of focal length F_0 as a function of NI/SQRT irritant factor (VR) for lenses at a constant acceleration voltage V_r=10kV, for the three lenses L1, L2, and L3

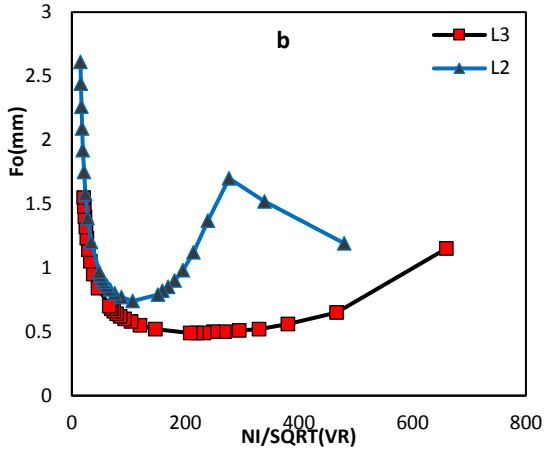

Fig. (6) Variation of focal length F_0 as a function of NI/SQRT irritant factor (VR) for lenses at a constant acceleration voltage V_r=10kV, (b) for the two lenses L2, and L3

The basics of this research is to design a strong objective lens with a short focal length, and from the last figure, the figure was divided into a and b for magnification and clarification of the difference between the lenses. It was found that the best uniform behavior obtained was for the L3 lens, which has the lowest value of the focal length F_0.

Figures (7-10) show the relationship between the spherical and chromatic aberration coefficients, respectively, of the designed lenses as a function of the acceleration voltage when excited by a constant NI = 4800 (A.T).

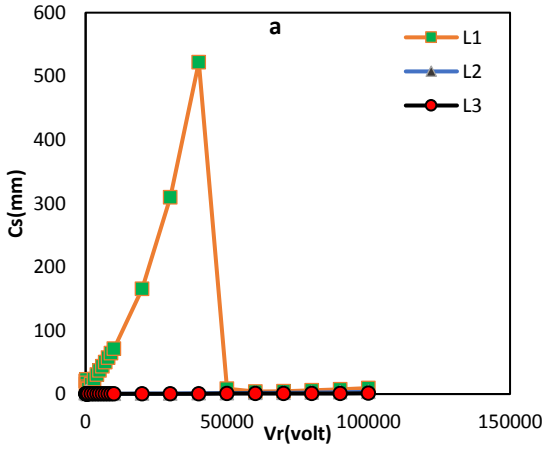

Fig. (7) Variation of spherical aberration as a function of the acceleration voltage when excited at a constant NI = 4800 (A.T), (a) for the three lenses L1, L2, and L3

Figures (11) and (12) show the change of the focal length F_o as a function of the acceleration voltage Vr for lenses L1, L2, L3 at constant excitation NI = 4800 (A.T). Figure (12) shows the change of the focal length as a function of the acceleration voltage when excited at a constant NI = 4800 (A.T) (b) for the two lenses L2, L3.

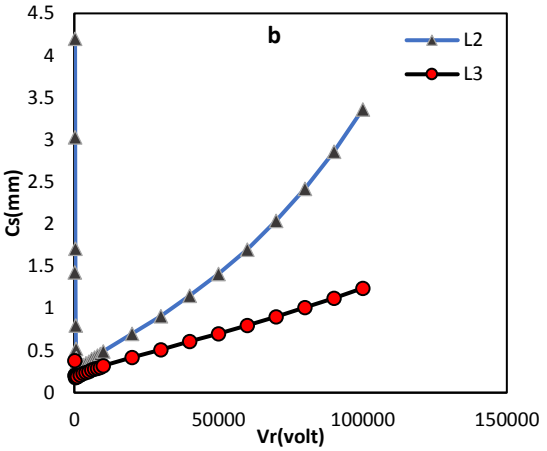

Fig. (8) Variation of spherical aberration as a function of the acceleration voltage when excited at a constant NI = 4800 (A.T), (b) for the two lenses L2, and L3

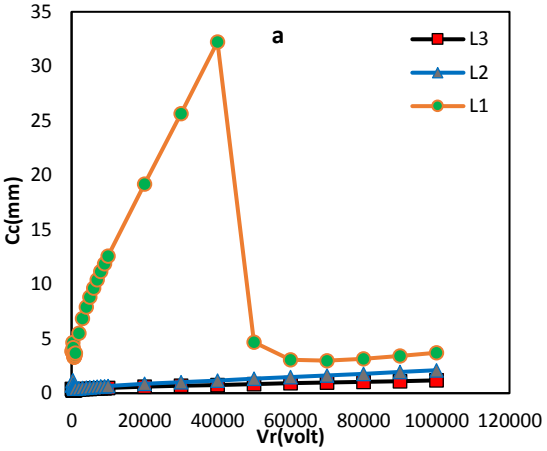

Fig. (9) Variation of chromatic aberration as a function of the acceleration voltage when excited at a constant NI=4800 (A.T), for the three lenses L1, L2, and L3

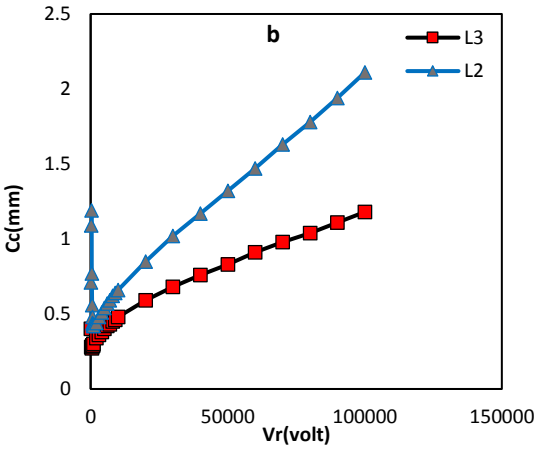

Figure (10) Variation of chromatic aberration as a function of the acceleration voltage when excited at a constant NI=4800 (A.T), (b) for the two lenses L2, and L3

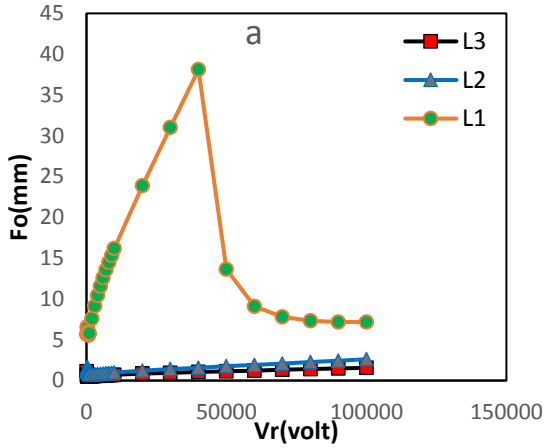

Fig. (11) Variation of the focal length as a function of the acceleration voltage when excited at a constant NI = 4800 (A.T), for the three lenses L1, L2, and L3

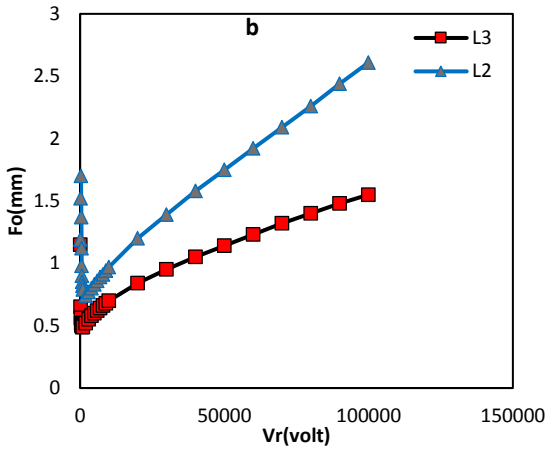

Fig. (12) Variation of the focal length as a function of the acceleration voltage when excited at a constant NI = 4800 (A.T), (b) for the two lenses L2, and L3

4. Conclusions

The symmetrical immersed magnetic objective lens, symbolized by L3, achieved the best results from the three proposed designs because it had the lowest values of the focal length that corresponded to the highest values in the analysis, and it had the lowest value for the spherical and chromatic aberration coefficients at a fixed value of the irritant factor (NI=4800 A.t).The change of the pole shape and the position of the pole head of the immersion magnetic lens directly affects the focal properties of the magnetic lens. L3 immersed magnetic objective lens has a maximum value of the axial magnetic flux density distribution ($B_{z.max}$ = 1.32 T) at the site (z=1mm) when the lens is excited (NI=4800 A.t).

References

[1] S.A. Sultan and A.I. Alabdullah, "Effect of pole face thickness on magnetization of the single-pole magnetic lens", *Rafidain J. Sci.*, 29(4) (2020) 44-52.

[2] H.S. Hasan, S.A. Obaid and M.S. Erhayief, "Recent Development-2 of CADTEL Software: The Optimum Conditions of Scherzer Imaging in the Electron Magnetic Lenses," *Iraqi J. Sci.*, ?? (2022) 131-148.

[3] H.S. Hasan, S.A. Obaid and M.S. Erhayief, "Munro's Electron Beam Software MEBS," Report, MEBS Ltd. (London, 2011).

[4] A.E Al-Abdullah, "The Electron Optical Properties of the Round Magnetic Electron Lens," *Rafidain J. Sci.*, 17(3) (2006) 59-69.

[5] B.F. Abd Alghane and A.K. Ahmad, "Design of symmetric magnetic lenses with optimum operational conditions," *Al-Nahrain J. Sci.*, 24(1) (2021) 30-38.

[6] M. Szilagyi, **"Electron and Ion Optics"**, Springer Science & Business Media (2012).

[7] J. Podbrdský, "High current density magnetic electron lenses in modern electron microscopes," *Scan. Electron Microsc.*, 1986(3) (1986) p. 8.

[8] P.W. Hawkes, **"Magnetic Lens Theory",** in Magnetic Electron Lenses, Springer (1982) 1-56.

[9] J. Pawley and H. Schatten, **"Biological Low-Voltage Scanning Electron Microscopy"**, Springer (2007).

[10] T.M. Abbas and Q.A. Sahi, "Design and Study of The Optical Properties of Electromagnetic lenses Dual-polar analog using the program I", *J. Univ. Babylon Pure Appl. Sci.*, 25(6) (2017) 1991-1997.

[11] T. Mohsen and L. Merry, "Studying the Properties of the Magnetic Optical Lenses by Using Mathematical Functions", *Int. J. Eng. Res.*, 3(7) (2014) ??-??.

[12] R.Y.J. Al-Salih, "The Influence of Bores Diameter on the SEM's Objective Lens Properties", *Tikrit J. Pure Sci.*, 23(2) (2018) 107-113.

[13] R.Y.J. Al-Salih, A.I.M. Al-Abdulla and E.M.A. Alkattan, "Simple program for computing objective optical properties of magnetic lenses", *Int. J. Comput. Appl. Technol.*, 66(3-4) (2021) 254-259.

[14] M.K. Al-Shammari, "Design and Improving the Optical Properties of a Magnetic Unipolar lens and Studying Its Geometric Parameters and Subjugation", MSc thesis, Tikrit University (2022) (not published).

IRAQI JOURNAL OF APPLIED PHYSICS LETTERS
EDITORIAL BOARD

COPYRIGHT RELEASE FORM

IRAQI JOURNAL OF
APPLIED PHYSICS LETTERS (IJAPLett)

We, the undersigned, the author/authors of the article titled

……
……
……
……
……
……
……

that is submitted to the Iraqi Journal of Applied Physics Letters (IJAPLett) for publication, declare that we have neither taken part or full text from any published work by others, nor presented or published it elsewhere in any other journal. We also declare transferring copyrights and conduct of this article to the Iraqi Journal of Applied Physics Letters (IJAPLett) after accepting it for publication.

The authors will keep the following rights:

1. Possession of the article such as patent rights.
2. Free of charge use of the article or part of it in any future work by the authors such as books and lecture notes after informing IJAP editorial board.
3. Republishing the article for any personal purposes of the authors after taking journal permission.

To be signed by all authors:

Signature:……..date: ……
Printed name: ……

Signature:……..date: ……
Printed name: ……

Signature:……..date: ……
Printed name: ……

Correspondence author:……...
……
Address:……
……
Telephone:……..……..email: ……

Note: Complete and sign this form and mail it to the below address with your finally revised manuscript

The Iraqi Journal of Applied Physics Letters
ISSN (Print): 1999-656x, ISSN (Online): 2309-1673
www.iraqiphysicsjournal.com
Email: editor@iraqiphysicsjournal.com
Email: editor_ijap@yahoo.co.uk
Email: ijap.editor@gmail.com

IRAQI JOURNAL OF APPLIED PHYSICS LETTERS
Volume (5) Issue (2) April-June 2022

CONTENTS

The *Iraqi Journal of Applied Physics Letters (IJAPLett)* is a peer reviewed journal of high quality devoted to the publication of original research papers from applied physics and their broad range of applications. IJAPLett publishes quality original research letters in physics and its applications in the broadest sense. It is intended that the journal may act as an interdisciplinary forum for physics and its applications. Innovative applications and material that brings together diverse areas of physics are particularly welcome. IJAPLett aims to disseminate knowledge; provide a learned reference in the field; and establish channels of communication between academic and research experts, policy makers and executives in industry, commerce and investment institutions. IJAPLett is a quarterly specialized periodical dedicated to publishing original letters in: Applied & Nonlinear Optics, Applied Mechanics & Thermodynamics, Digital & Optical Communications, Electronic Materials & Devices, Laser Physics & Applications, Plasma Physics & Applications, Quantum Physics & Spectroscopy, Semiconductors & Optoelectronics, Solid State Physics & Applications, Alternative & Renewable Energy, and Environmental Science & Technology.

Sponsored and Published by
Iraqi Society for Alternative and Renewable Energy Sources and Techniques

Co-published by
American Quality for Scientific Publishing